Article

Intra- and Intermolecular NMR Studies on the Activation of Arylcyclometallated Hafnium Pyridyl-Amido Olefin Polymerization Precatalysts

Cristiano Zuccaccia, Alceo Macchioni, Vincenzo Busico, Roberta Cipullo, Giovanni Talarico, Francesca Alfano, Harold W. Boone, Kevin A. Frazier, Phillip D. Hustad, James C. Stevens, Paul C. Vosejpka, and Khalil A. Abboud

J. Am. Chem. Soc., **2008**, 130 (31), 10354-10368 • DOI: 10.1021/ja802072n • Publication Date (Web): 10 July 2008

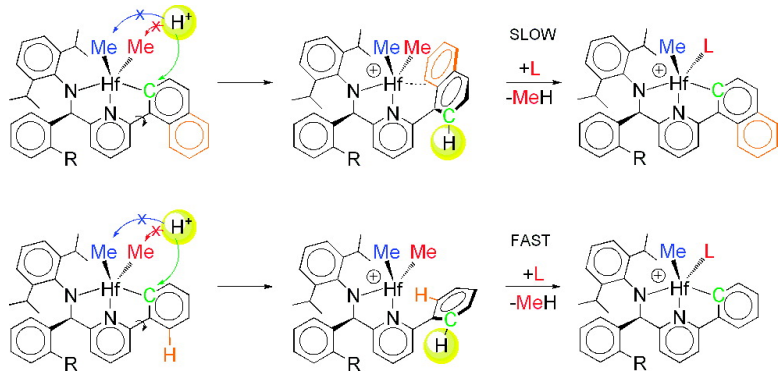

J|A|C|S
ARTICLES

Published on Web 07/10/2008

Intra- and Intermolecular NMR Studies on the Activation of Arylcyclometallated Hafnium Pyridyl-Amido Olefin Polymerization Precatalysts

Cristiano Zuccaccia,[†] Alceo Macchioni,*[,†] Vincenzo Busico,[‡] Roberta Cipullo,[‡] Giovanni Talarico,[‡] Francesca Alfano,[‡] Harold W. Boone,[§] Kevin A. Frazier,[||] Phillip D. Hustad,[§] James C. Stevens,[§] Paul C. Vosejpka,[||] and Khalil A. Abboud[⊥]

Department of Chemistry, University of Perugia, Via Elce di Sotto, 8, 06123 Perugia, Italy, Department of Chemistry, University of Napoli, Via Cintia, 80126 Napoli, Italy, The Dow Chemical Company, 2301 North Brazosport Boulevard, B-1814, Freeport, Texas 77541, The Dow Chemical Company, 1776 Building, Midland, Michigan 48674, and Department of Chemistry, University of Florida, Gainesville, Florida 32611

Received March 25, 2008; E-mail: alceo@unipg.it

Abstract: Pyridyl-amido catalysts have emerged recently with great promise for olefin polymerization. Insights into the activation chemistry are presented in an initial attempt to understand the polymerization mechanisms of these important catalysts. The activation of C_1-symmetric arylcyclometallated hafnium pyridyl-amido precatalysts, denoted $Me_2Hf\{N^-,N,C^-\}$ (**1**, aryl = naphthyl; **2**, aryl = phenyl), with both Lewis ($B(C_6F_5)_3$ and $[CPh_3][B(C_6F_5)_4]$) and Brønsted ($[HNR_3][B(C_6F_5)_4]$) acids is investigated. Reactions of **1** with $B(C_6F_5)_3$ lead to abstraction of a methyl group and formation of a single inner-sphere diastereoisomeric ion pair $[MeHf\{N^-,N,C^-\}][MeB(C_6F_5)_3]$ (**3**). A 1:1 mixture of the two possible outer-sphere diastereoisomeric ion pairs $[MeHf\{N^-,N,C^-\}][B(C_6F_5)_4]$ (**4**) is obtained when $[CPh_3][B(C_6F_5)_4]$ is used. $[HNR_3][B(C_6F_5)_4]$ selectively protonates the aryl arm of the tridentate ligand in both precatalysts **1** and **2**. A remarkably stable $[Me_2Hf\{N^-,N,C_2\}][B(C_6F_5)_4]$ (**5**) outer-sphere ion pair is formed when the naphthyl substituent is present. The stability is attributed to a hafnium/η^2-naphthyl interaction and the release of an eclipsing H−H interaction between naphthyl and pyridine moieties, as evidenced through extensive NMR studies, X-ray single crystal investigation and DFT calculations. When the aryl substituent is phenyl, $[Me_2Hf\{N^-,N,C_2\}][B(C_6F_5)_4]$ (**10**) is originally obtained from protonation of **2**, but this species rapidly undergoes remetalation, methane evolution, and amine coordination, giving a diastereomeric mixture of $[MeHf\{N^-,N,C^-\}NR_3][B(C_6F_5)_4]$ (**11**). This species transforms over time into the trianionic-ligated $[Hf\{N^-,C^-,N,C^-\}NR_3][B(C_6F_5)_4]$ (**12**) through activation of a C−H bond of an amido-isopropyl group. In contrast, ion pair **5** does not spontaneously undergo remetalation of the naphthyl moiety; it reacts with NMe_2Ph leading to $[MeHf\{N^-,N\}NMe_2C_6H_4][B(C_6F_5)_4]$ (**7**) through ortho-metalation of the aniline. Ion pair **7** successively undergoes a complex transformation ultimately leading to $[Hf\{N^-,C^-,N,C^-\}NMe_2Ph][B(C_6F_5)_4]$ (**8**), strictly analogous to **12**. The reaction of **5** with aliphatic amines leads to the formation of a single diastereomeric ion pair $[MeHf\{N^-,N,C^-\}NR_3][B(C_6F_5)_4]$ (**9**). These differences in activation chemistry are manifested in the polymerization characteristics of these different precatalyst/cocatalyst combinations. Relatively long induction times are observed for propene polymerizations with the naphthyl precatalyst **1** activated with $[HNMe_3Ph][B(C_6F_5)_4]$. However, no induction time is present when **1** is activated with Lewis acids. Similarly, precatalyst **2** shows no induction period with either Lewis or Brønsted acids. Correlation of the solution behavior of these ion pairs and the polymerization characteristics of these various species provides a basis for an initial picture of the polymerization mechanism of these important catalyst systems.

Introduction

An important class of C_1-symmetric (pyridyl-amido)Hf(IV)-based olefin polymerization catalysts was recently discovered by means of high throughput screening technologies.[1–3] The general structure of the neutral precatalysts is shown in Chart 1. Performance of these catalysts is unique and truly remarkable. In particular, highly isotactic high molecular weight propene homopolymers and copolymers can be produced at very high reaction temperatures, enabling their production in solution process technologies.[4] In ethylene/1-alkene copolymerizations, higher 1-alkenes (such as 1-hexene or 1-octene) are effectively incorporated. Last but not least, under proper conditions, the active species are amenable to fast and reversible trans-alkylation with main group metal−alkyls (such as ZnR_2); this can be used advantageously in the preparation of olefin block copolymers via "chain shuttling".[5]

[†] University of Perugia.
[‡] University of Napoli.
[§] The Dow Chemical Company, Texas.
[||] The Dow Chemical Company, Michigan.
[⊥] University of Florida.

10.1021/ja802072n CCC: $40.75

From the structural point of view, precatalysts shown in Chart 1 are unconventional and peculiar in several respects. A most notable feature is the ortho-metalation of the aryl substituent on the pyridine ring, resulting in tridentate ligation of the pyridyl−amido moiety and a slightly distorted trigonal bipyramidal Hf coordination.[3] A second important structural element is a stereogenic carbon linking the pyridyl and the amido fragments; albeit remote from the active site, this chiral center appears to influence enantioselectivity in the insertion of prochiral 1-alkenes.[3] A third feature is the high Lewis acidity of the 5-coordinate 12e$^-$ Hf(IV) center, which is further enhanced upon activation with cocatalysts.

Despite the well-defined nature of the precatalysts (Chart 1), catalysts derived from them exhibit polymerization characteristics indicative of multiple catalytic species. For example, ethylene copolymers from these precatalysts normally display multimodal molecular weight and composition distributions.[6] To gain understanding of the mechanism of these important and intriguing systems, we undertook a comprehensive experimental and computational investigation of their reactivity. Integrated results of intra- and intermolecular solution NMR studies, X-ray crystallography, density functional theory (DFT) calculations, and ad hoc (poly-)-insertion experiments revealed a complex and in some respects surprising picture. In this manuscript, we describe interactions of precatalyst with various cocatalysts. A subsequent report will focus on chain initiation reactions. While the activation of precatalysts shown in Chart 1 with Lewis acids is in line with the normal observations described for other precatalysts for olefin polymerization,[7–9] an additional layer of complexity appears when the activation is carried out with Brønsted acids. This is substantially due to the presence of the cyclometalated aryl moiety that provides an alternative site for protonation with respect to other dimethyl precatalysts.

Chart 1

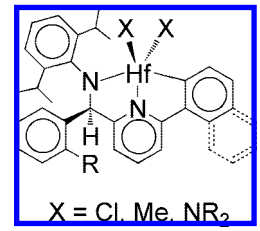

Scheme 1. Hafnium Pyridyl−Amido Dimethyl Complexes[a]

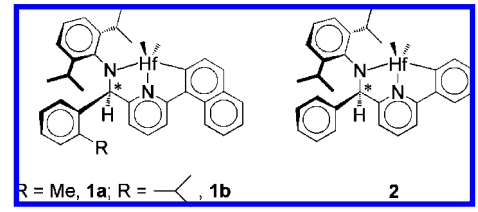

[a] The stereoisomer with (*R*)-Configuration at C* is shown although racemic mixtures were used.

Scheme 2. Activation Chemistry of **1** with $B(C_6F_5)_3$ to Give Inner-Sphere Ion Pairs **3**

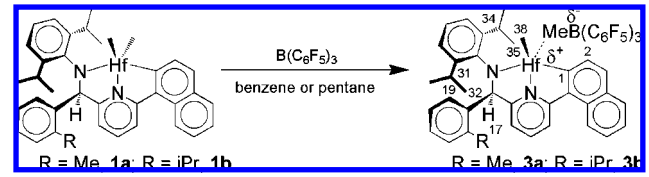

Results and Discussion

In an attempt to understand the complex polymerization characteristics exhibited by these catalyst systems, we initially set out to characterize the ion pairs resulting from reaction of the dimethyl derivatives **1** and **2** (Scheme 1 and Figure S1 of the Supporting Information) with typical cocatalysts. We decided not to explore methylalumoxane (MAO) because of its complex solution NMR spectra and instead focused on two well-known Lewis acids, $B(C_6F_5)_3$ and $[CPh_3][B(C_6F_5)_4]$, and the Brønsted acid $[HNMe_2Ph][B(C_6F_5)_4]$. Characterization of the resulting ion pairs in solution was performed using an array of NMR techniques and is described in detail as follows. For the discussion, the structure of the ligand is abbreviated as $\{N^-,N,C^-\}$ to indicate a tridentate species with a neutral Hf-pyridyl bond (N) and anionic Hf-amide (N^-) and Hf-carbon (C^-) bonds. Similarly, the ligand in a dimethyl complex where the aryl has been protonated would be designated $\{N^-,N,C_2\}$.

Activation with Lewis Acids. a. $B(C_6F_5)_3$. The reaction of $B(C_6F_5)_3$ with complexes **1a** and **1b** leads to the selective abstraction of the methyl group Me-37, which lies in the pseudo-cis position with respect to H-17, and formation of inner-sphere ion pairs (ISIPs) **3a** and **3b**, as shown in Scheme 2. The broad B−Me resonance observed around 3 ppm in the ^{1}H NMR spectrum provides evidence of methide abstraction; this resonance is typical of a $MeB(C_6F_5)_3^-$ counterion partially coordinated to the metal.[10] Consistent with this partial coordination,

(1) (a) Boussie, T. R.; Diamond, G. M.; Goh, C.; Hall, K. A.; LaPointe, A. M.; Leclerc, M. K.; Lund, C.; Murphy, V. U.S. Patent Appl. 0135722 A1, 2006. (b) Boussie, T. R.; Diamond, G. M.; Goh, C.; Hall, K. A.; LaPointe, A. M.; Leclerc, M. K.; Lund, C.; Murphy, V. U.S. Patent 7,018,949, 2006. (c) Boussie, T. R.; Diamond, G. M.; Goh, C.; LaPointe, A. M.; Leclerc, M. K.; Lund, C.; Murphy, V. U.S. Patent 6,750,345, 2004. (d) Boussie, T. R.; Diamond, G. M.; Goh, C.; Hall, K. A.; LaPointe, A. M.; Leclerc, M. K.; Lund, C.; Murphy, V. U.S. Patent 6,713,577, 2004. (e) Boussie, T. R.; Diamond, G. M.; Goh, C.; Hall, K. A.; LaPointe, A. M.; Leclerc, M. K.; Lund, C.; Murphy, V. U.S. Patent 6,706,829, 2004. (f) Boussie, T. R.; Diamond, G. M.; Goh, C.; Hall, K. A.; LaPointe, A. M.; Leclerc, M. K.; Lund, C.; Murphy, V. PCT Int. Appl. WO 046249, 2002. (g) Boussie, T. R.; Diamond, G. M.; Goh, C.; Hall, K. A.; LaPointe, A. M.; Leclerc, M. K.; Lund, C.; Murphy, V. PCT Pat. Appl. WO 038628, 2002.
(2) Boussie, T. R.; Diamond, G. M.; Goh, C.; Hall, K. A.; LaPointe, A. M.; Leclerc, M. K.; Lund, C.; Murphy, V.; Shoemaker, J. A. W.; Tracht, U.; Turner, H.; Zhang, J.; Uno, T.; Rosen, R. K.; Stevens, J. C. *J. Am. Chem. Soc.* **2003**, *125*, 4306.
(3) Boussie, T. R.; Diamond, G. M.; Goh, C.; Hall, K. A.; LaPointe, A. M.; Leclerc, M. K.; Murphy, V.; Shoemaker, J. A. W.; Turner, H.; Rosen, R. K.; Stevens, J. C.; Alfano, F.; Busico, V.; Cipullo, R.; Talarico, G. *Angew. Chem., Int. Ed.* **2006**, *45*, 3278.
(4) (a) Arriola, D. J.; Bokota, M.; Timmers, F. J. PCT Int. Appl. WO 026925 A1, 2004. (b) Frazier, K. A.; Boone, H.; Vosejpka, P. C.; Stevens, J. C. U.S. Patent Appl. 0220050 A1, 2004. (c) Tau, L.-M.; Cheung, Y. W.; Diehl, C. F.; Hazlitt, L. G. U.S. Patent Appl. 0087751 A1, 2004. (d) Tau, L.-M.; Cheung, Y. W.; Diehl, C. F.; Hazlitt, L. G. U.S. Patent Appl. 0242784 A1, 2004. (e) Coalter, J. N., III; Van Egmond, J. W.; Fouts, L. J., Jr.; Painter, R. B.; Vosejpka, P. C. PCT Int. Appl. WO 040195 A1, 2003. (f) Stevens, J. C.; Vanderlende, D. D. PCT Int. Appl. WO 040201 A1, 2003.
(5) Arriola, D. J.; Carnahan, E. M.; Hustad, P. D.; Kuhlman, R. L.; Wenzel, T. T. *Science* **2006**, *312*, 714.
(6) Froese, R. D. J.; Hustad, P. D.; Kuhlman, R. L.; Wenzel, T. T. *J. Am. Chem. Soc.* **2007**, *129*, 7831.
(7) Chen, E. Y.-X.; Marks, T. J. *Chem. Rev.* **2000**, *100*, 1391.
(8) Britovsek, G. P.; Gibson, V. C.; Wass, D. F. *Angew. Chem., Int. Ed.* **1999**, *38*, 428.
(9) (a) Macchioni, A. *Chem. Rev.* **2005**, *105*, 2039. (b) Bochmann, M. *J. Organomet. Chem.* **2004**, *689*, 3982.
(10) Axenov, K. V.; Martti, K.; Markku, L.; Repo, T. *Organometallics* **2005**, *24*, 1336.

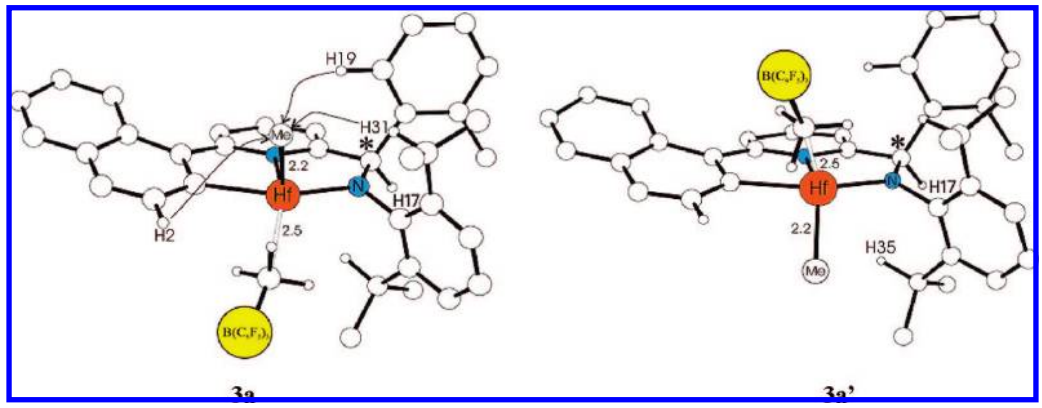

Figure 1. Full QM-optimized structures of the ion pairs **3a** with the coordination of the anion in a pseudo-cis position with respect to H17 (**3a**) and in pseudo-trans position (**3a′**). For the sake of visibility, some H atoms are omitted and the $[MeB(C_6F_5)_3]^-$ anion is reported with the methyl group in scale and $B(C_6F_5)_3$ moiety as a ball. Distances are in Å.

a $\Delta\delta$(*m*-F, *p*-F) of 4.7 ppm is observed in the ^{19}F NMR spectrum.[11] The selectivity of the Me-abstraction is indicated by the observation of intense NOEs between the remaining Hf-Me38 group and H2, H19, and H31, while no interaction is observed with H35. The anion coordination in a pseudo-cis position with respect to H17 is supported by the ^{19}F,^{1}H HOESY NMR experiment;[12] the *o*-F shows strong interionic interactions with H2, H34, H32, and H35, while none is observed with H31. In addition, very weak interionic contacts are present between cationic H32 and H35 resonances and the *m*-F, in agreement with an orientation in which the anion steadily points Me-37 toward the Hf atom.[13,14] An exchange NOE cross peak between the broad B−Me resonance and Me38 is also observed in a phase-sensitive ^{1}H-nuclear Overhauser effect spectroscopy (NOESY) experiment. This suggests that the other diastereoisomeric ion pair, with $MeB(C_6F_5)_3^-$ in a pseudo-trans position with respect to H17, is accessible, but its abundance is under the threshold of detection of the NMR spectroscopy. As a consequence, **3a**,**b** are thermodynamically favored with respect to the other possible diastereoisomers.

The activation reaction of **1a** (Scheme 2) was also evaluated theoretically using full quantum mechanical (QM) calculations (see Supporting Information for details). The calculated enthalpy for the methide abstraction reaction is −17 kcal/mol. As expected, correcting for solvation effects with the COSMO model[15] does not change the ΔH value significantly (−16.6 kcal/mol), as there is no net charge separation on either side of the reaction. The calculated value is in line with the few experimental values reported for metallocene systems (e.g., Cp_2ZrMe_2 precatalyst, where a ΔH value of −23.1 kcal/mol was measured by titration calorimetry)[16] and with similar computations done by Ziegler et al.[17] In agreement with NOE NMR results, the ion pair with the anion in the pseudo-cis position with respect to H17 (Figure 1, **3a**) is more stable compared to the one in the pseudo-trans position (Figure 1, **3a′**) by 0.7 kcal/mol.[18]

Scheme 3. Activation Chemistry of **1b** with $[CPh_3][B(C_6F_5)_4]$, Including Significant Chemical ^{13}C Shift Values

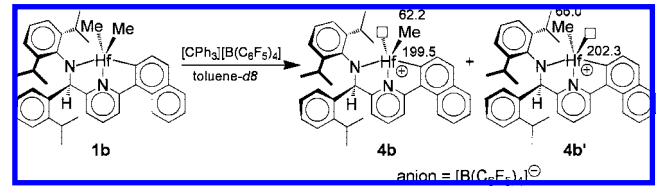

Ion pairs **3a** and **3b** have limited stability at room temperature in benzene or toluene solution under an inert atmosphere. After a few hours, they begin to decompose through a process involving both single and double C_6F_5-transfers[19] forming $MeB(C_6F_5)_2$ and $Me_2B(C_6F_5)$.[20,21]

b. $[CPh_3][B(C_6F_5)_4]$. The reaction of complex **1b** with 1 equiv of $[CPh_3][B(C_6F_5)_4]$ in toluene-d_8 proceeds quantitatively, giving two diastereoisomeric ion pairs **4b** and **4b′** in approximately a 1:1 ratio (Scheme 3). Although the complete assignment of the NMR resonances of **4b** and **4b′** is hampered by extensive overlapping and the 1:1 abundance ratio, a partial assignment can be performed upon inspection of the low temperature ^{1}H rotating frame Overhauser effect spectroscopy (ROESY) spectrum (Supporting Information).

(11) The value of Δd(*m,p*-F) (^{19}F NMR) is a good probe of coordination of $MeB(C_6F_5)_3^-$ to cationic d^0 metals (values of 3−6 ppm indicate coordination; <3 ppm indicates non-coordination). See : Horton, A. D.; de With, J. *Organometallics* **1997**, *16*, 5424, and references therein.
(12) Macchioni, A. *Eur. J. Inorg. Chem.* **2003**, 195, and references therein.
(13) Correa, A.; Cavallo, L. *J. Am. Chem. Soc.* **2006**, *128*, 10952.
(14) Zuccaccia, C.; Stahl, N. G.; Macchioni, A.; Chen, M.-C.; Roberts, J. A.; Marks, T. J. *J. Am. Chem. Soc.* **2004**, *126*, 1448.
(15) Pye, C. C.; Ziegler, T. *Theor. Chim. Acta* **1999**, *101*, 396.
(16) (a) Deck, P. A.; Marks, T. J. *J. Am. Chem. Soc.* **1995**, *117*, 6128. (b) Deck, P. A.; Beswick, C. L.; Marks, T. J. *J. Am. Chem. Soc.* **1998**, *120*, 1772.
(17) Xu, Z.; Vanka, K.; Firman, T.; Michalak, A.; Zurek, E.; Zhu, C.; Ziegler, T. *Organometallics* **2002**, *21*, 2444.
(18) This value does not take into account the entropic effect. In fact, for the structure **3a** we found two stable species with the same energy which differs for the relative configuration of the $B(C_6F_5)_3$ moiety. This is not true for **3a′**.
(19) For some examples of C_6F_5-transfer to the metal see:(a) Phomphrai, K.; Fenwick, A. E.; Sharma, S.; Fanwick, P. E.; Caruthers, J. M.; Delgass, W. N.; Abu-Omar, M. M.; Rothwell, J. P. *Organometallics* **2006**, *25*, 214. (b) Metcalfe, R. A.; Kreller, D. I.; Tian, J.; Kim, H.; Taylor, N. J.; Corrigan, J. F.; Collins, S. *Organometallics* **2002**, *21*, 1719. (c) Woodman, T. J.; Thornton-Pett, M.; Hughes, D. L.; Bochmann, M. *Organometallics* **2001**, *20*, 4080. (d) Guerin, F.; Stewart, J. C.; Beddie, C.; Stephan, D. W. *Organometallics* **2000**, *19*, 2994–3000. (e) Scollard, J. D.; McConville, D. H.; Rettig, S. J. *Organometallics* **1997**, *16*, 1810. (f) Yang, X. M.; Stern, C. L.; Marks, T. J. *J. Am. Chem. Soc.* **1994**, *116*, 10015. For a recent theroretical work see: (g) Wondimagegn, T.; Xu, Z.; Vanka, K.; Ziegler, T. *Organometallics* **2004**, *23*, 3847, and references therein.
(20) Krempner, C.; Ko1ckerling, M.; Reinke, H.; Weichert, K. *Inorg. Chem.* **2006**, *45*, 3203.
(21) Although structures of the hafnium-containing decomposition products were difficult to assign, the appearance of high frequency resonances in the ^{19}F NMR spectrum (around−120 ppm) suggests the formation of Hf-C_6F_5 fragments : Tonzetich, Z. J.; Schrock, R. R. *Polyhedron* **2006**, *25*, 469.

Scheme 4. Activation Chemistry of **1a**,**b** with $[HNMe_2Ph][B(C_6F_5)_4]$

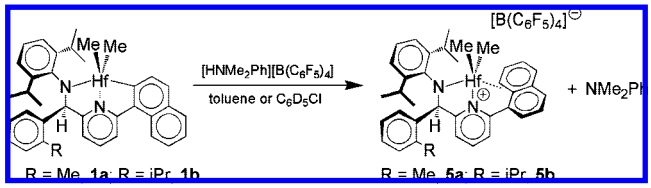

Exchange cross peaks are observed in the ^{1}H NOESY spectrum recorded at room temperature between resonances of **4b** and **4b′**, indicating that, as for **3a**,**b**, the observed abundance ratio is dictated by thermodynamics. The observation of a 1:1 ratio for **4b** and **4b′** suggests that the vacant coordination site, derived from the abstraction of the methyl group, remains substantially unoccupied and can be "kinetically" stabilized by the bulky 2,6-diisopropylphenyl moiety or involved in weak interactions with solvent or counterion. In all cases, **4b** and **4b′** have to be considered outer-sphere ion pairs (OSIPs).[22]

The results of theoretical investigations (see section 1.1 and Figure S2 of the Supporting Information) are again consistent with these observations. In fact, the energy of the two diastereoisomeric ion pairs is substantially the same (ΔE < 0.2 kcal/mol), indicating no diastereoselectivity for the activation process.[23]

In contrast to **3a** and **3b**, the mixture **4b**/**4b′** is stable in toluene-d_8 solution for days at room temperature in the absence of light. Exposure to sunlight or the use of more polar and coordinating solvents, such as C_6D_5Cl, causes rapid decomposition to a complex mixtures of species.

Activation with Brønsted Acids. a. Naphthyl Precatalysts, 1a,b. As mentioned above, the activation of **1** and **2** with Lewis acids is not unusual compared to that of other dialkyl precatalysts. However, the chemistry observed in combination with Brønsted acids is strikingly different and makes this catalyst family unique. The reaction of **1a** and **1b** with $[HNMe_2Ph][B(C_6F_5)_4]$ proceeds with selective protonation of the Hf−napthyl bond and formation of **5a** and **5b** OSIPs (Scheme 4) rather than liberation of methane as is typical of other dimethyl precatalysts.

Protonation of the Hf−naphthyl bond is demonstrated by the disappearance of the high-frequency ^{13}C NMR resonance (around 200 ppm), and the appearance of an additional aromatic C−H moiety. The naphthyl orientation in solution after demetalation is deduced by analyzing the ^{1}H NOESY NMR spectrum (Figure 2). The following selective contacts are present: H37 with H7 (strong), H6 (strong), H8 (medium), and H5 (medium); H38 with H1 (medium), H2 (medium), and H3 (weak); H1 with H12; H8 with H34. The average distance in solution between H34 and H8, estimated by semiquantitative analysis of NOESY data, is 2.94 Å.[24] These observations

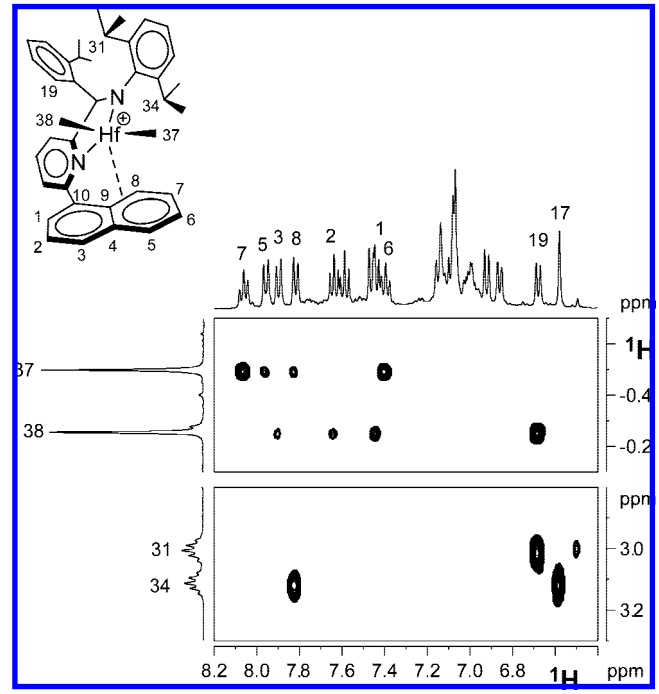

Figure 2. Two sections of the ^{1}H NOESY NMR spectrum of complex **5b** (C_6D_5Cl, 298 K). The upper section shows the selective interactions of H37 with H7, H6, H5, and H8 and those of H38 with H19, H1, H2, and H3, while, in the lower section, the selective and strong interaction between H34 and H8 is illustrated.

Table 1. ^{13}C NMR Chemical Shifts for the Naphthyl Protons of Complexes **1** and **5**−**9**

	1a	1b	5a	5b	6a	7b	8b	9b
C1	206.7	206.8	133.6	132.9	122.7	127.6	206.1	202.2
C2	134.8	134.8	131.9	131.3	130.2	127.7	132.1	131.5
C3	130.6	130.5	134.0	133.3	136.8	134.1	∼128.5	131.2
C4	136.4	136.4	138.7	137.9	136.8		135.4	135.8
C5	130.6	130.6	137.9	137.2	131.2	130.5	129.9	130.0
C6	126.2	126.2	131.7	131.0	133.4	130.1	127.0	127.6
C7	127.6	127.6	143.9	143.0	133.0	130.1	∼128.5	128.9
C8	127.3	124.9	114.1	113.3	124.6	124.1	123.7	123.7
C9	131.3	131.4	128.6	127.7	129.3		130.8	129.8
C10	144.7	144.7	130.7	129.9	133.4		142.3	144.5

indicate that the C_6H_4 moiety of the napthyl group is oriented toward H34 as shown in Figure 2. In agreement, both resonances of the terminal Hf−Me groups appear at lower frequency compared to the neutral precatalysts (H37, $\delta_H = -0.50$ ppm in **5a** and −0.49 ppm in **5b**; H38, $\delta_H = -0.29$ ppm in **5a** and −0.25 ppm in **5b**), due to the shielding effect exerted by the naphthyl group. In addition, variations in the ^{13}C NMR shifts of naphthyl carbons of **1a**,**b** and **5a**,**b** suggest an electronic interaction between the naphthyl unit and the metal center (Table 1).

Differences in the ^{13}C chemical shift of C7−C10 are comparable or even higher than those observed for benzene or toluene coordination to a group 4 d^0 metal[25] and for unsymmetrical (η^1-fashion) olefin coordination in metallocene-based

(22) Schrock, R. R.; Casado, A. L.; Goodman, J. T.; Liang, L-C.; Bonitatebus, P. J. J.; Davis, W. M. *Organometallics* **2000**, *19*, 5325.

(23) The heterolytic separation of the [MeHf{N-,N,C-}][$B(C_6F_5)_4$] ion pair with the solvent inclusion is calculated lower than the one for [MeHf{N-,N,C-}][$MeB(C_6F_5)_3$] ion pair (see Supporting Information).

(24) Integration of NOESY cross peaks in the initial rate approximation (see Neuhaus, D.; Williamson, M. *The Nuclear Overhauser Effect in Structural and Conformational Analysis*, Wiley-VCH: New York, 2000; Chapter 4) gave the following relative values: $A_{H7/H8} = 1$; $A_{H34/H17} = 1.06$; $A_{H34/H8} = 0.35$. The distance between H7 and H8, 2.47 Å, (Zuccaccia, C.; Bellachioma, G.; Cardaci, G.; Macchioni, A. *J. Am. Chem. Soc.* **2001**, *123*, 11020. was used as reference distance, affording 2.44 and 2.94 Å for H34/H17 and H34/H8 distances, respectively.

(25) (a) Deckers, P. J. W.; van der Linden, A. J.; Meetsma, A.; Hessen, B. *Eur. J. Inorg. Chem.* **2000**, 929. (b) Lancaster, S. J.; Robinson, O. B.; Bochmann, M.; Coles, S. J.; Hursthouse, M. B. *Organometallics* **1995**, *14*, 2456.

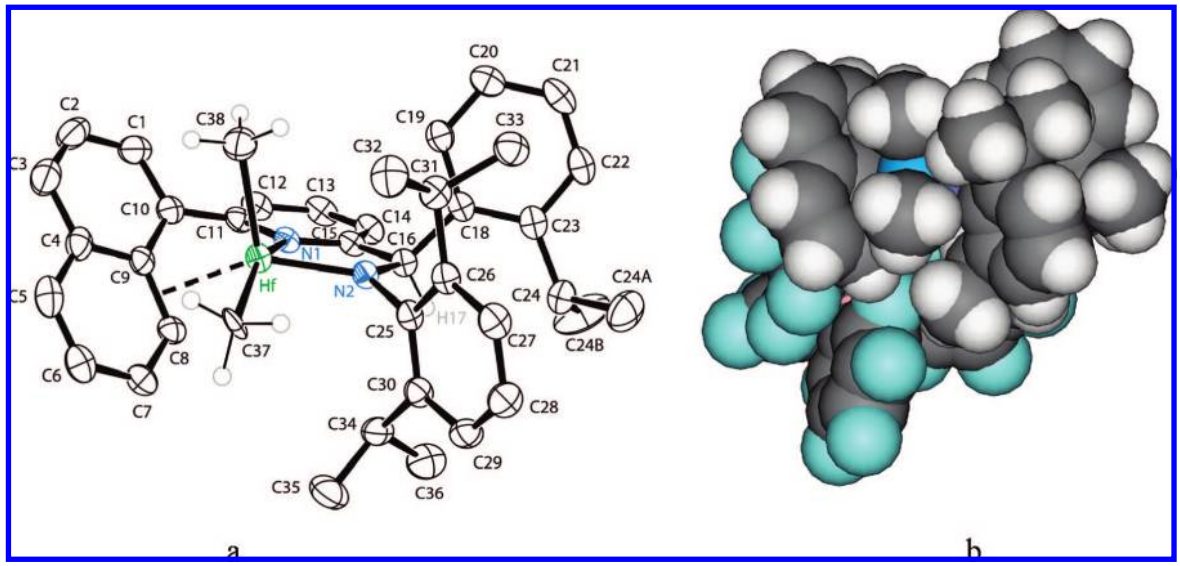

Figure 3. X-ray crystallographic characterization of **5b**, displaying (a) an ORTEP drawing of the cationic portion of the ion pair and (b) a CPK representation of the ion pair in almost the same orientation, displaying the shortest Hf−B distance (7.230 Å) in the solid state. Some hydrogen atoms are omitted in both drawings for the sake of clarity.

systems.[26] It appears clear that C8, which shows the largest decrease in chemical shift, is involved in naphthyl coordination (Table 1). Both the Hf−naphthyl interaction and the release of the strong H−H eclipsing interaction between H8 and H12, originally present in the neutral precatalyst (vide infra), impart stability to **5a** and **5b** ion pairs, which do not show any sign of decomposition in toluene after 10 days at room temperature.

A ^{19}F,^{1}H HOESY experiment allows location of the anion with respect to the cation. In this case, both the *o*-F and *m*-F interact with selected cationic resonances in a fashion typical of OSIPs;[14] the *o*-F and *m*-F correlate with H14 (strong), H8 (strong), H13 (medium), H12 (medium), H7 (weak), H3 (weak), H5 (weak), H1 (weak), H34 (weak), H36 (weak), H35 (weak), and H17 (very weak). These results indicate that, in solution, the anion is positioned close to the pyridyl-amido ligand, partly shifted on the side of H17, and far away from the two terminal methyl groups.

The solid state and theoretical structures of **5b** are consistent with the solution structure determined by NMR investigations. An ORTEP drawing of the cationic portion of the species is shown in Figure 3a. The naphthyl group is oriented toward H34, as deduced in solution through NOE experiments, and has a H8/H34 distance equal to 2.93 Å, in excellent agreement with NOE results (2.94 Å). The closest distances from naphthyl carbons to the hafnium center are observed for C8 (2.612 Å) and C9 (2.737 Å), while the C8−C9 centroid is closer (2.576 Å), suggesting an η^2-coordination of the naphthyl group. The overall geometry around the metal center can be considered a markedly distorted trigonal bipyramid having the pyridine nitrogen N1 and C37 in apical positions, approaching a square pyramid having C38 in the vertex.

The results of theoretical calculations are consistent with the NOE results and the solid state structure **5b**. In fact, the lowest minima structure corresponds to **5b**; however, a structure with similar energy (<0.3 kcal/mol) showing a short C1−Hf distance was also found, indicating an accessible restricted rotation of the naphthyl group along the C10−C11 bond (see Figure S3 of Supporting Information).

As far as cation−anion interactions are concerned, there are six anions surrounding each cation in the solid state. The one displaying the shortest Hf−B distance (7.230 Å, Figure 3b) is located close to the backbone of the pyridyl-amido ligand, on the side of H17, in good agreement with the average solution interionic OSIP structure determined by ^{19}F,^{1}H HOESY experiments.

To determine whether and under what conditions the remetalation of **5** takes place, the reactivities of ion-pairs **5a** and **5b** were investigated under conditions similar to those employed in typical polymerizations. These experiments included investigations at higher reaction temperatures and combinations with other reagents that can be present during polymerizations, such as Lewis and Brønsted acids and other nucleophiles. This chemistry is described below and summarized in Scheme 5.

Increasing the temperature of solutions of **5a**,**b** in different solvents leads to evolution of CH_4 and decomposition both in the absence and presence of an excess of $AlMe_3$. Addition of a stoichiometric amount of $B(C_6F_5)_3$ to a benzene-d_6 solution of **5a** does not produce any immediate detectable reaction, but extensive decomposition is observed after two days.[27] No indication of naphthyl remetalation is observed in either case.

The reaction of **5a** with a stoichiometric amount of $[HNMe_2Ph][B(C_6F_5)_4]$ leads to selective protonation of Me37, evolution of CH_4, and occupation of the generated coordination site by NMe_2Ph to afford ion pair **6a** (Scheme 5, pathway A). Consistently, the remaining Hf-Me38 methyl group shows intense NOEs with H31 and H32, indirectly demonstrating the selective protonation of Me37. The NOE contacts of H8 with H12 and H38 with H1 and H2 indicate that the naphthyl moiety is now almost perpendicularly oriented to the pyridyl ring and is no longer coordinated to the Hf center. This decoordination is also supported by the chemical shift values of C7−C10, which are similar to those of **1a**,**b** (Table 1). Interestingly, the coordinated NMe_2Ph shows seven ^{1}H resonances, five aromatic and two aliphatic, indicating a restricted rotation around the

(26) (a) Stoebenau, E. J.; Jordan, R. F. *J. Am. Chem. Soc.* **2006**, *128*, 8638. (b) Stoebenau, E. J.; Jordan, R. F. *J. Am. Chem. Soc.* **2004**, *126*, 11170.

(27) The ^{1}H NMR spectrum allows us to individuate some resonances of $MeB(C_6F_5)_2$ and $Me_2B(C_6F_5)$ (d_H = 0.96 and 1.33 ppm, respectively), while the appearance of high frequency (around−120 ppm) resonances in the ^{19}F NMR spectrum suggests the formation of Hf-C_6F_5 fragments.

Scheme 5. Reactions of **5a**,**b** with Possible Species Present in Polymerization Reactions

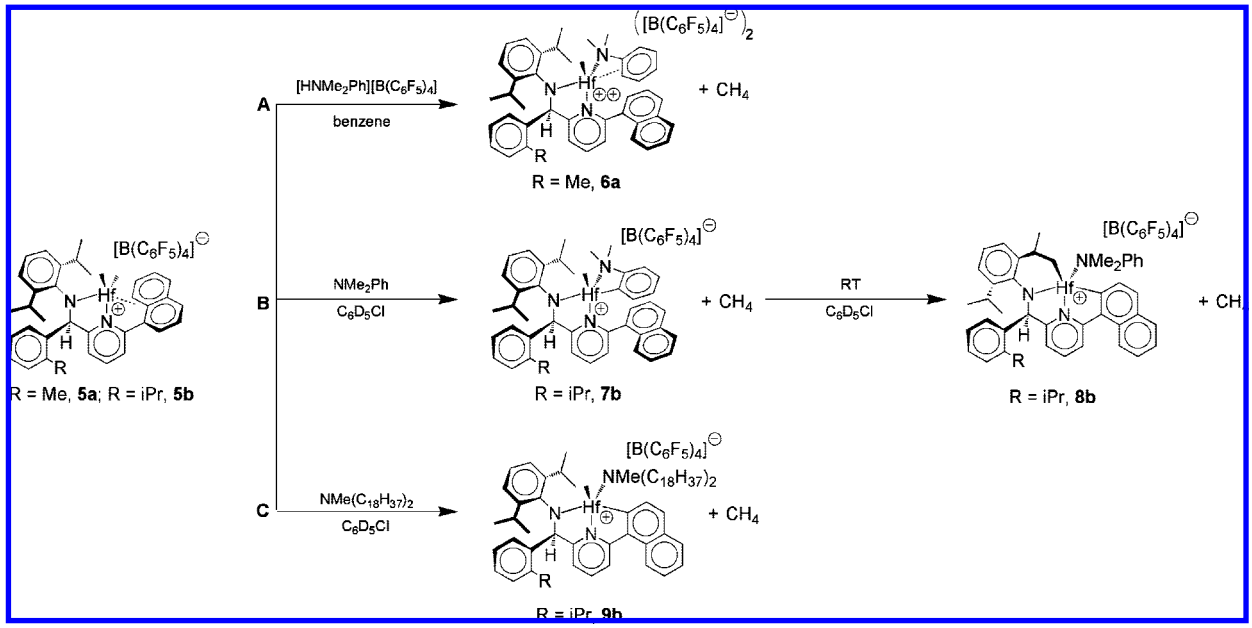

N−C*ipso* bond. The *o*-H/H39 and *o*-H′/H40 NOEs are of comparable intensity (Figure 4) and are in agreement with an almost perpendicular orientation of the aniline ring with respect to the plane containing the C*ipso*-N bond that bisects the Me−N−Me angle. The presence of Overhauser contacts of *o*-H with H38, H3 and H2, *m*-H with H2, H3, and H1, *o*-H′ with H35, and, most notably, *p*-H with H8 and H34 (Figure 4) shows that the phenyl ring of the aniline is oriented toward the backbone of the ligand. This orientation may be due to a partial electronic interaction of the aniline arene ring with Hf, similar to that observed in complex **5a** and **5b** for the naphthyl unit. ^{13}C NMR data shows evidence of this through a high frequency shift for *m*-C and C*ipso* (ca. 6 and ca. 2 ppm, respectively) and a significant low frequency shift for the *p*-C (ca. 8 ppm). Moreover, despite its bicationic nature, complex **6a** is rather stable in aromatic nonchlorinated solvents such as a benzene/1,2-$F_2C_6H_4$ mixture, but it slowly decomposes in CD_2Cl_2 at room temperature.[28] The ^{19}F NMR spectrum of **6a** displays the typical resonances for uncoordinated $[B(C_6F_5)_4]^-$ anions, while the ^{19}F,^{1}H HOESY spectrum displays rather unselective interionic contacts as expected for a bicationic species.

Another species that is surely present in solution when **1a**,**b** are activated with $[HNMe_2Ph][B(C_6F_5)_4]$ is NMe_2Ph. To determine if the presence of this aniline may facilitate the η^2-decoordination and metalation of the naphthyl moiety, the reaction of **5b** with NMe_2Ph was investigated by an in situ activation of **1b** with $[HNMe_2Ph][B(C_6F_5)_4]$ in C_6D_5Cl at room temperature. As hypothesized, decoordination of the naphthyl moiety and metalation does occur, but the latter does not involve the naphthyl moiety. Instead, a C−H activation occurs at the *o*-carbon of aniline,[29,30] leading to the formation of **7b** (Scheme 5, pathway B). The release of a terminal methyl group is indicated by CH_4 evolution and the final presence of a single Hf−Me resonance ($\delta_H = 1.40$; $\delta_C = 66.7$ ppm). The metalation of an *o*-carbon of aniline is evidenced by the observation of two NMe_2 resonances ($\delta_H = 2.20$ and 0.86 ppm; $\delta_C = 46.4$ and 41.1 ppm) that show strong NOEs, of similar intensities, with the doublet at 6.70 ppm, assigned to the only ortho-proton of the aniline present in the ^{1}H NMR spectrum. The ^{1}H COSY spectrum (Supporting Information) undoubtedly indicates that this *o*-H resonance is part of a scalarly coupled four-spin system lacking one proton in the aniline ring. Aniline ortho metalation is further supported by a high frequency resonance in the ^{13}C NMR spectrum ($\delta_C = 192.9$ ppm) that also has long-range correlations with *m*-H′, *p*-H, and *o*-H in the ^{1}H, ^{13}C, HMBC spectrum.

The three-dimensional structure of the cationic portion of **7b** can be inferred by analyzing the ^{1}H NOESY and ^{1}H ROESY spectra. The Hf−Me moiety remains in a pseudo-trans position with respect to H17 (NOEs with H1, H2, H19, and H31). The carbon and nitrogen arms of the cyclometallated aniline are in pseudo-trans[31] and pseudo-cis[32] positions with respect to the pyridine nitrogen, respectively. The NOE interaction between

(28) The decomposition product could not be completely characterized; ^{1}H NMR data are consistent with formation of a mixed-methyl-chloride hafnium species having a structure similar to **5a**, together with $[ClCD_2NMe_2Ph][B(C_6F_5)_4]$. ^{1}H NMR for the Hf species (CD_2Cl_2, 298 K, *J* values in Hz): d 8.71 (d, $^3J_{HH} = 8.4$, H5), 8.67 (td, $^3J_{HH} = 7.4$, $^4J_{HH} = 1.1$, H7), 8.58 (d, $^3J_{HH} = 8.4$, H3), 8.42 (t, $^3J_{HH} = 8.0$, H13), 8.33 (dd, $^3J_{HH} = 8.4$, $^4J_{HH} = 7.3$, H2), 8.21 (dd, $^3J_{HH} = 7.3$, $^4J_{HH} = 1.1$, H1), 8.14 (d, $^3J_{HH} = 8.0$, H12), 8.12 (td, $^3J_{HH} = 7.3$, $^4J_{HH} = 1.1$, H6), 8.05 (d, $^3J_{HH} = 7.8$, H8), 7.45 (d, $^3J_{HH} = 8.0$, H14), 7.32 (m, H28 and H29), 7.20 (m, H20 and H21), 7.10 (dd, $^3J_{HH} = 7.2$, $^4J_{HH} = 1.7$, H22), 7.00 (dd, $^3J_{HH} = 7.3$, $^4J_{HH} = 2.0$, H27), 6.87 (dd, $^3J_{HH} = 7.2$, $^4J_{HH} = 1.6$, H19), 6.51 (s, H17), 3.14 (sept, $^3J_{HH} = 6.8$, H34), 2.85 (sept, $^3J_{HH} = 6.8$, H31), 1.78 (s, H24), 1.57 (d, $^3J_{HH} = 6.8$, H36), 1.55 (d, $^3J_{HH} = 6.8$, H35), 0.90 (d, $^3J_{HH} = 6.8$, H32), 0.08 (s, H38), 0.04 (d, $^3J_{HH} = 6.8$, H33). ^{1}H NMR for $[ClCD_2NMe_2Ph][B(C_6F_5)_4]$ (CD_2Cl_2, 298 K): 7.72 (m, 3 protons), 7.42 (m, 2 protons), 3.48 (s, 6 protons).

(29) For examples of amine activation, see: (a) Krut'ko, D. P.; Borzov, M. V.; Kirsanov, R. S.; Churakov, A. V.; Kuz'mina, L. G. *J. Organomet. Chem.* **2005**, *690*, 3243. (b) Pflug, J.; Bertuleit, A.; Kehr, G.; Fröhlich, R.; Erker, G. *Organometallics* **1999**, *18*, 3818.

(30) For examples of *N*,*N*-bis-alkyl-aniline ortho-metallation see: (a) Solé, D.; Vallverdù, L.; Solans, X.; Font-Bardìa, M.; Bonjock, J. *J. Am. Chem. Soc.* **2003**, *125*, 1587. (b) Drost, C.; Hitchcock, P. B.; Lappert, M. F. *Angew. Chem., Int. Ed.* **1999**, *38*, 1113. (c) Edema, J. J. H.; Gambarotta, S.; Meetsma, A.; Speks, A. L. *Organometallics* **1992**, *11*, 2452.

(31) H39 shows NOE peaks with H1, H2, and H3 while H40 shows an NOE with H8.

(32) *m*-H′, *p*-H and *o*-H interact with H35.

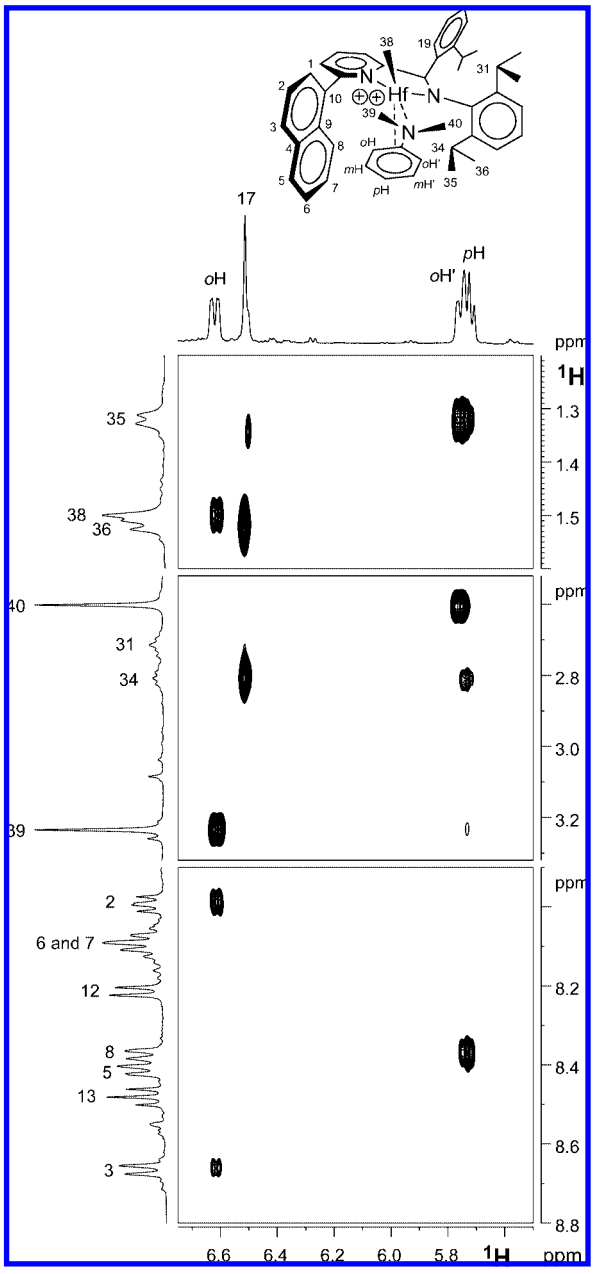

Figure 4. Three sections of the ^{1}H ROESY NMR spectrum of complex **6a** (CD_2Cl_2 217 K), showing Overhauser contacts between the aniline aromatic protons (*o*-H, *o*-H′, and *p*-H) and protons of the pyridyl-amido ligand. The contact between *p*-H and H34 (middle section) is of particular interest.

H12 and H8 and the chemical shift values of C7 and C8 indicate that the naphthyl moiety points away from the Hf center (Table 1). The structure obtained by DFT calculations, with its distorted square pyramid geometry, is in agreement with ^{1}H NOESY and ^{1}H ROESY results (Figure 5).

In C_6D_5Cl at room temperature, **7b** slowly undergoes a remarkably complex but clean transformation into **8b** (Scheme 5, pathway B). This transformation formally involves the decyclometalation of the aniline, metalation of both the naphthyl and an isopropyl group,[33] and methane evolution. Methane is clearly visible in ^{1}H NMR spectrum. As an indication of isopropyl metalation, only five isopropyl doublets were present in the aliphatic region of the ^{1}H NMR spectrum. Two new multiplets, each integrating for one proton, appeared at δ_H = 1.40 ppm (H32a) and δ_H = 0.78 ppm (H32b). These resonances showed a scalar correlation with H31 in the ^{1}H-COSY spectrum, and H32a and H32b correlated with the same carbon resonance (δ_C = 81.2 ppm) in the ^{1}H,^{13}C HMQC spectrum (Figure 6A). Naphthyl metalation is verified by the observation of a two spin system in the aromatic region of the ^{1}H NMR spectrum and a long-range correlation with the carbon resonance at δ_C = 206.1 ppm in the ^{1}H,^{13}C HMBC spectrum (Figure 6B). Finally, the demetalation of aniline is supported by the observation of magnetically equivalent ortho and meta resonances and the integration consistent with five aromatic protons. As far as the stereochemistry of **8b** is concerned, the observation of selective and relatively strong dipolar interactions between H17 and H34 and H36 indicate that the unaltered isopropyl group resides in the relative pseudo-cis position with respect to H17, while, consequently, C32 remains in the pseudo-trans relative position. DFT calculations on the stereochemistry of **8b** confirmed that structure **8b** is 1.5 kcal/mol more stable than **8b′**, the structure with the isopropyl group in the relative pseudo-trans position with respect to H17 (see Figure S5 of the Supporting Information).

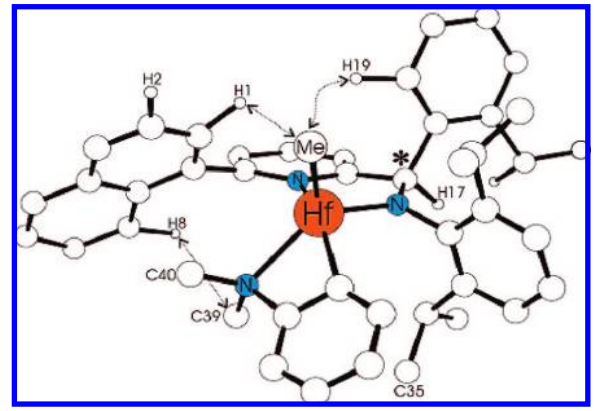

Figure 5. Full QM optimized structures of complexes **7b**. For the sake of visibility, H atoms are omitted with the exception of the ones discussed in the text. The arrows display some important NOEs observed in solution. The stereogenic carbon center linking the pyridyl and the amido fragment is indentified with a star.

Because activation of aromatic amines competes with cyclometalation of the naphthyl moiety, we decided to test the reactivity of **5** with aliphatic amines. According to Scheme 5, pathway C, when 1 equiv of $CH_3N(C_{18}H_{37})_2$ is added to a C_6D_5Cl solution of **5b**, a release of CH_4 and formation of complex **9b** is observed. The reaction proceeds cleanly at room temperature and is complete in one hour. Evidence of naphthyl metalation is provided by the appearance of a carbon resonance at δ_C = 202 ppm having long-range correlations with both H2 and H3 in the ^{1}H,^{13}C HMBC spectrum. The selective NOE interaction between the Hf−Me group and H31 again indicates that the protonation occurs stereoselectively at C37 of the starting ion pair **5b**. Finally, coordination of the amine is demonstrated by the presence of two separate resonances for the diastereotopic α-CH_2 carbons (δ_C = 54.4 and 53.9 ppm) and the presence of a strong NOE cross peak between the

(33) (a) For similar isopropyl C-H activation reactions, see for example: Otten, E.; Dijkstra, P.; Visser, C.; Meetsma, A.; Hessen, B. *Organometallics* **2005**, *24*, 4374. (b) Volkis, V.; Nelkenbaum, E.; Lisovskii, A.; Hasson, G.; Semiat, R.; Kapon, M.; Botoshansky, M.; Eishen, M.; Eisen, M. S. *J. Am. Chem. Soc.* **2003**, *125*, 2179. (c) Tempel, D. J.; Johnson, L. K.; Huff, R. L.; White, P. S.; Brookhart, M. *J. Am. Chem. Soc.* **2000**, *122*, 6686.

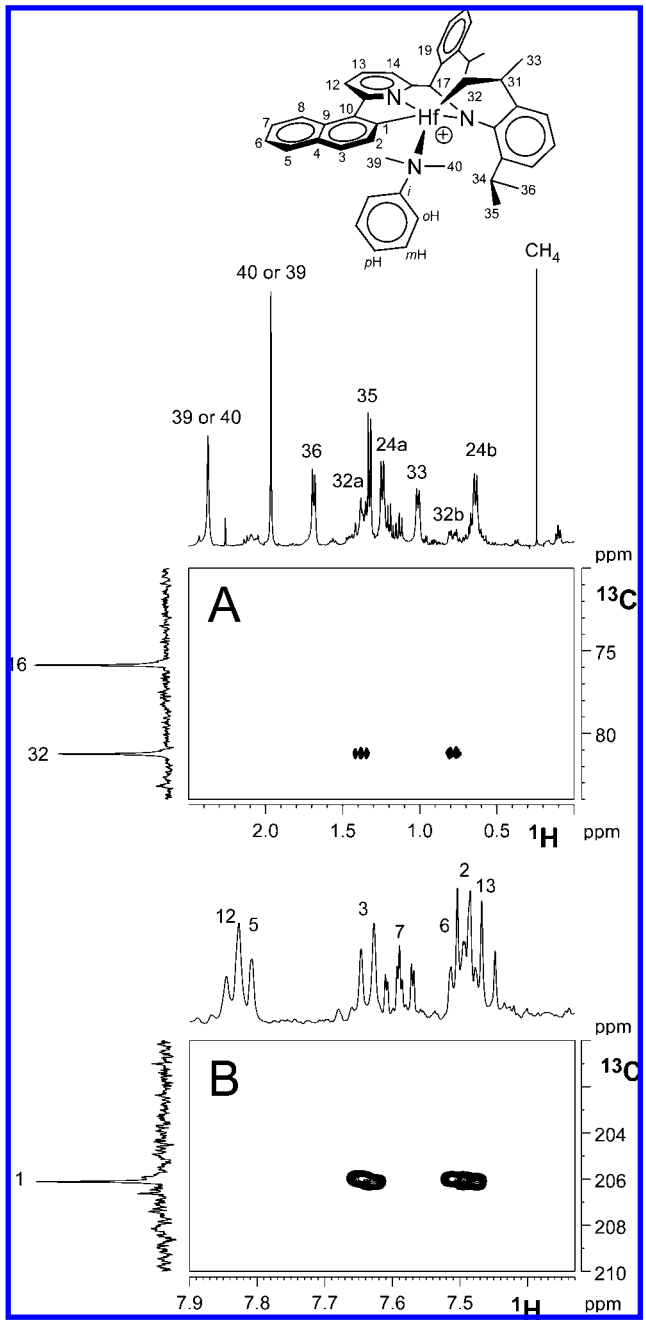

Figure 6. Correlation spectra for complex **8b** (C_6D_5Cl, 298 K), including (A) a section of the $^1H,^{13}C$ HMQC NMR spectrum showing the connection between the methylene carbon C32 and the two diasterotopic hydrogens (H32a and H32b) and (B) a section of the $^1H,^{13}C$ HMBC NMR spectrum showing the long-range correlation between the metallated carbon (C1) and aromatic H2 and H3 protons.

N−Me group and H2. The ^{19}F NMR spectrum shows resonances corresponding to an uncoordinated anion, while the $^{19}F,^1H$ HOESY experiment shows that the anion prefers to pair with the cation from the side of the coordinated amine. Both the *o*-F and *m*-F resonances of the anion show interactions with the N−Me and the $-(CH_2)_n-$ resonances of the aliphatic chains.

b. Phenyl Precatalyst, 2. From the results reported above, it is clear that the naphthyl unit plays a crucial role in determining the reactivity of complexes **1a** and **1b** with Brønsted acids. Structural information, both in solution (NMR) and solid state (X-ray diffraction), consistently indicates that the initially formed cationic species (**5a** and **5b**) arising from selective protonation

Scheme 6. Activation Chemistry of **2** with $[HNMe_2Ph][B(C_6F_5)_4]$

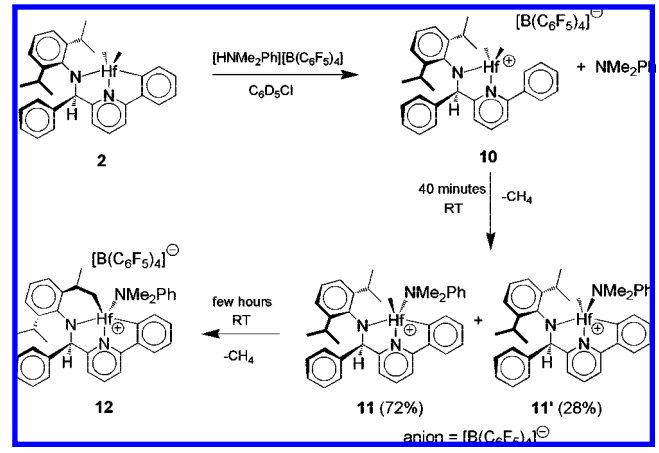

at the aromatic ring may be kinetically and/or thermodynamically stabilized by a Hf-η^2-naphthyl interaction. With the aim of better understanding the impact of the naphthyl functionality, we investigated the stoichiometric reaction of the corresponding precatalyst **2**, bearing a phenyl instead of a naphthyl substituent, with $[HNMe_2Ph][B(C_6F_5)_4]$ in C_6D_5Cl at room temperature. We also explored the thermodynamics of the reaction with computational calculations.

The reaction of **2** with $[HNMe_2Ph][B(C_6F_5)_4]$ is much faster than that of **1b**, proceeding to completion in 20 min instead of 56 h. As with precatalysts **1a**,**b**, the phenyl group is initially protonated to give monocationic species **10** (Scheme 6). However, before it is completely formed, **10** begins to transform through phenyl metalation with methane evolution and aniline coordination (Supporting Information). The reaction gives a mixture of the diastereoisomeric monomethyl ion pairs **11** and **11′** in a 72:28 molar ratio. When the reaction is carried out at low temperature, an almost complete conversion of **2** into **10** is observed, suggesting that protonation proceeds regioselectively at the Hf−phenyl bond. In a few hours at room temperature, the **11/11′** mixture leads to complex **12** as a consequence of C−H activation of the isopropyl moiety with concurrent methane evolution (Scheme 6).

Complex **12** is analogous to **8b**, and similar rationale can be followed to obtain the complete resonance assignments and determine its three-dimensional structure through NOE studies. The ^{19}F NMR spectrum is typical of an uncoordinated $B(C_6F_5)_4^-$, while several cross peaks with both aliphatic and aromatic resonances are present in the $^{19}F,^1H$ HOESY spectrum (Figure 7). The absence of fluorine interactions with H32a, H32b, H31, and H33 suggests that the anion approaches the cation from the side occupied by the coordinated aniline.

The main difference in the reactivity of dimethyl precatalysts **1** and **2** toward the Brønsted acid $[HNMe_2Ph][B(C_6F_5)_4]$ is a consequence of the higher stability of the protonated naphthyl complex (**5**) with respect to the analogous phenyl one (**10**). The latter is the kinetic product of the protonation process that readily undergoes phenyl metalation with methane evolution to give a monomethyl cation stabilized by the coordination of aniline (**11** and **11′**). On the contrary, the η^2-naphthyl interaction with hafnium stabilizes species **5** such that it first undergoes binding of the aniline followed by (probably fast) cyclometalation with methane evolution to give **7b**. Both **11/11′** and **7b** evolve to

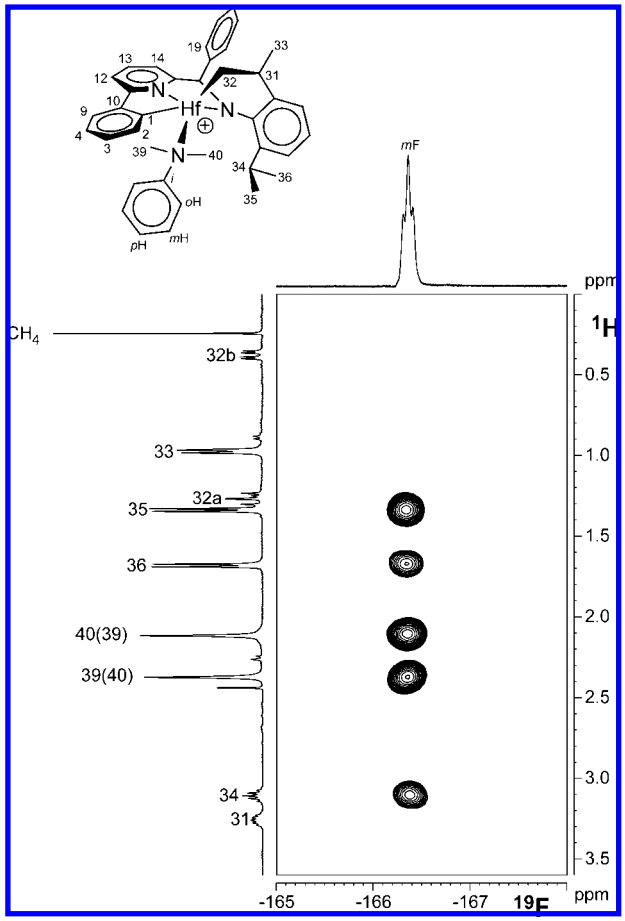

Figure 7. A section of the $^{19}F,^{1}H$ HOESY NMR spectrum (C_6D_5Cl, 298 K) of ion pairs **12**. No interaction between the *m*-F and H31, H32a, H32b, and H33 is observed.

thermodynamically stable complexes (**8b** and **12**)[34] derived from the activation of a C−H bond of the isopropyl group. This process is more complex in the case of **7b** since aniline decyclometalation and naphthyl metalation must both occur. **7b** may initially undergo an exchange of a proton between the naphthyl and aniline moieties leading to an intermediate analogous to **11/11′** that successively transforms into **8b**. An additional explanation for the different reactivity of dimethyl precatalysts **1** and **2** toward the Brønsted acid was offered by DFT calculations on the thermodynamic cycle for the reactions going from **5** to **8b** (system **1**) and from **10** to **12** (system **2**, see Figure S6 of Supporting Information for the relative structures). In fact, computations show gains in the energy of 18.4 and 26.7 kcal/mol for **1** and **2**, respectively, for these processes. This difference of about 9 kcal/mol is attributed to the steric hindrance between the naphthyl and pyridine rings in the ortho-metallated species, which forces the naphthyl to have an orientation out of the Hf-pyridine plane (Figure 8); this constraint is not present for the system bearing the phenyl group (Figure 8). A comparable distortion is surely present in metallated precatalysts **1a** and **1b**, and the release of the steric congestion after protonation/demetalation of the naphthyl functionality may substantially contribute to the overall stability of ion pairs **5a** and **5b**.

(34) Reactions of **8b** and **12** with molecular hydrogen at room temperature did not afford any reaction after several hours.

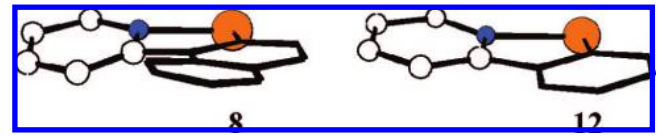

Figure 8. Lateral view of the full QM optimized **8** and **12** structures. For the sake of visibility, H atoms are omitted and the ligands have been reduced to the pyridine and naphthyl and phenyl rings. Distortion of the naphthyl ring compared to the phenyl one is evidenced.

Table 2. Polymerization of 1-Octene at Room Temperature Using Precatalysts **1b** and **2**[a]

run	precatalyst	precatalyst (μmol)	activator	T_{max}[b] (°C)	t_{max}[c] (min)
1	**1b**	10	$[CPh_3][B(C_6F_5)_4]$	117.3	0.87
2	**1b**	10	$[HNMe_2Ph][B(C_6F_5)_4]$	126.5	9.80
3	**1b**	5	$[HNMe_2Ph][B(C_6F_5)_4]$	122.2	15.30
4	**1b**	2	$[HNMe_2Ph][B(C_6F_5)_4]$	91.7	81.90
5	**2**	10	$[CPh_3][B(C_6F_5)_4]$	110.3	5.97
6	**2**	10	$[HNMe_2Ph][B(C_6F_5)_4]$	107.6	8.23

[a] General reaction conditions: [1-octene] = 3.2 M, 1 equiv activator. [b] T_{max} = maximum temperature observed during reaction. [c] t_{max} = time required to reach the maximum reaction temperature.

Correlations with the Catalytic Behavior in α-Olefin Polymerization. In principle, ortho-aryl-metallated $[\{N^-,N,C^-\}HfMe]^+$ and nonmetallated $[\{N^-,N\}HfMe_2]^+$ cations can both represent active species in catalytic olefin polymerization. These species both have at least one Hf−C σ-bond and one coordination vacancy on Hf for the incoming monomer. The factual observation of M_w/M_n values >2.0 (Schulz−Flory distribution) for ethene/1-alkene copolymers obtained with a number of (pyridyl-amido)Hf-based catalysts is indeed an indication of a nonsingle-center catalyst nature. This may (also) be traced to the fact that $[\{N^-,N,C^-\}HfMe]^+$ cations undergo monomer insertion into the Hf-aryl σ-bond with a corresponding in situ ligand modification and diversification.[6] To explore these possibilities, we carried out a number of polymerization experiments in the presence of catalyst systems obtained by reacting precatalysts **1b** and **2** with stoichiometric amounts of $[CPh_3][B(C_6F_5)_4]$ and $[HNMe_2Ph][B(C_6F_5)_4]$. In particular, we conducted polymerizations of 1-octene at room temperature, monitoring the exotherm produced by polymerization as an indication of the catalytic activity. We also performed polymerizations of propene at 50 °C under more controlled conditions to measure kinetic profiles from monomer uptake.

Polymerizations of 1-octene (Table 2) provide insight into the differences in activation chemistry of these complexes. Reactions with **1b** and **2** demonstrate large differences in the kinetic profiles generated with different types of cocatalysts (Figure 9). For both precatalysts, activation with $[CPh_3][B(C_6F_5)_4]$ results in an immediate increase in reaction temperature. The Brønsted acid $[HNMe_2Ph][B(C_6F_5)_4]$, however, produces a different response; the profiles from both **1b** and **2** show induction times consistent with slow activation processes. Precatalyst **2** has a shorter induction period than **1b**, consistent with the NMR observations that show the aryl metalation is much faster for phenyl derivatives. The duration of the induction period is also highly dependent on catalyst concentration. The time required (t_{max}) to reach the maximum reaction temperature (T_{max}) was extended from 9.8 to 81.9 min with a 5-fold decrease in concentration of **1b**. These results are all consistent with the activation processes observed by NMR.

Propene uptake curves from polymerizations conducted at 50 °C in toluene solution (Table 3 and Figure 10) are consistent with the above observations. For precatalyst **1b**, activation with

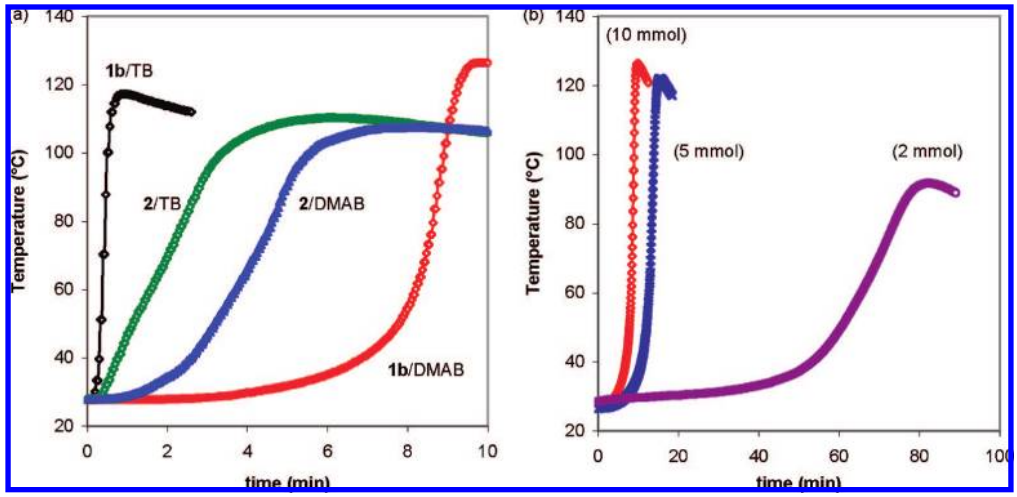

Figure 9. Temperature profiles from 1-octene polymerizations, including (a) **1b** and **2** activated with different cocatalysts (TB = $[CPh_3][B(C_6F_5)_4]$, DMAB = $[HNMe_2Ph][B(C_6F_5)_4]$), and (b) concentration effects with **1b**/DMAB.

Table 3. Polymerization of Propene at 50°C using Precatalysts **1b** and **2**[a]

run	precatalyst	precatalyst (μmol)	activator	t (min)	yield (mg)	[*mmmm*][b]
1	**1b**	0.010	$[Ph_3C][B(C_6F_5)_4]$	29	149	0.975
2	**1b**	0.050	$[HNMe_2Ph][B(C_6F_5)_4]$	50	150	0.970
3	**2**	0.010	$[Ph_3C][B(C_6F_5)_4]$	22	90	0.885
4	**2**	0.050	$[HNMe_2Ph][B(C_6F_5)_4]$	36	90	0.885

[a] General reaction conditions: p(propene) = 2.0 bar, 1.2 equiv. activator, 1.0 mM $Al(^iBu)_3$ as a scavenger. [b] Fraction of isotactic pentad in the polymer, measured by ^{13}C NMR.

$[CPh_3][B(C_6F_5)_4]$ resulted into practically immediate polymerization activity, whereas a long (ca. 20 min) induction period was observed upon activation with $[HNMe_2Ph][B(C_6F_5)_4]$. On the other hand, catalyst systems based on **2** behaved similarly with both $[CPh_3][B(C_6F_5)_4]$ and $[HNMe_2Ph][B(C_6F_5)_4]$ activation, with no appreciable induction. For each catalyst, a different choice of activator resulted in a different productivity at stationary state (ca. 5−10 times higher with $[CPh_3][B(C_6F_5)_4]$ than with $[HNMe_2Ph][B(C_6F_5)_4]$, possibly due to the coordinating ability of dimethylaniline), but had no measurable effects on the selectivity as identical polymer microstructures were observed by ^{13}C NMR.

On the basis of these polymerization results and on the precatalyst activation studies reported in the previous sections, we conclude that nonmetallated $[\{N^-,N\}HfMe_2]^+$ species **5a**,**b** and **10** are polymerization-inactive (or poorly active at most), and that the ortho-aryl-metalation is essential for (high) polymerization activity.

Conclusions and Perspectives

Because of the wealth of interesting polymerization characteristics displayed by hafnium pyridyl-amido complexes, we sought to gain a fundamental understanding of their activation and polymerization mechanisms. These studies have revealed that the unique catalytic properties displayed by these species are perhaps rivaled by the peculiarities observed in the activation chemistry. Treatment of these procatalysts with Lewis acids $B(C_6F_5)_3$ and $[CPh_3][B(C_6F_5)_4]$ reveals typical chemistry for such reactions, forming the expected ion pairs. However, activation of these precatalysts with Brønsted acids proceeds in a rather unusual way leading to complex, and aryl-dependent, subsequent rearrangements of the formed ion pairs. These reactions proceed initially with selective protonation of the aryl moiety, not the methyl moiety as typically observed for other dialkyl precatalysts (Scheme 7). In the case of naphthyl precatalysts **1**, protonation leads to an ion pair stabilized by an Hf-η^2-naphthyl interaction that slowly undergoes remetalation of the naphthyl moiety with methane evolution to form a single diastereoisomeric ion pair (Scheme 7). A nucleophile appears to be necessary to release the Hf-η^2-naphthyl interaction, allowing naphyl rotation and remetalation. The structural impossibility of stabilizing the protonated species, the lack of an eclipsing H−H interaction, and the statistically doubled possibility of activating an *o*-C−H bond makes the aryl remetalation much faster in the case of the phenyl precatalyst **2** (Scheme 7). Again, one diastereosomeric ion pair prevalently forms in these C_1-symmetric chiral complexes.

The parallelism between the ease of aryl-CH-activation of the dimethyl aryl-protonated species and the induction time observed in α-olefin polymerizations is consistent with previous conclusions that these species are more distant from the catalytically active species (if not altogether inactive) than the monomethyl aryl-metallated species generated by reaction with Lewis acids. It would be reasonable to conclude that the latter complexes were representative of the catalytically active species. While this work demonstrates the indispensability of the Hf−aryl carbon bond to the catalysis, it does not necessarily indicate that the aryl-metallated species are active polymerization catalysts. As if the mechanisms described above were not complex enough, it has been recently proposed that the first olefin insertion is more likely to occur into the Hf−aryl carbon bond instead of the Hf−methyl bond.[6] This mechanism, based on theoretical and experimental evidence, involves a very unusual modification of the ligand structure by monomer to give the highly active polymerization catalyst. Recent observations by Domski and Coates[35] and Hustad and co-workers,[36] who independently discovered that related achiral species give prevalently isotactic poly-(α-olefins) in spite of the C_s-symmetry of the precatalysts, also supports this mechanism. To understand the importance of this hypothesis of ligand modification by

(35) Domski, G. J.; Lobkovsky, E. B.; Coates, G. W. *Macromolecules* **2007**, *40*, 3510–3513.
(36) Hustad, P. D.; Froese, R. D. J.; Zuccaccia, C.; Macchioni, A.; Busico, V.; Cipullo, R.; Talarico, G. Unpublished results.

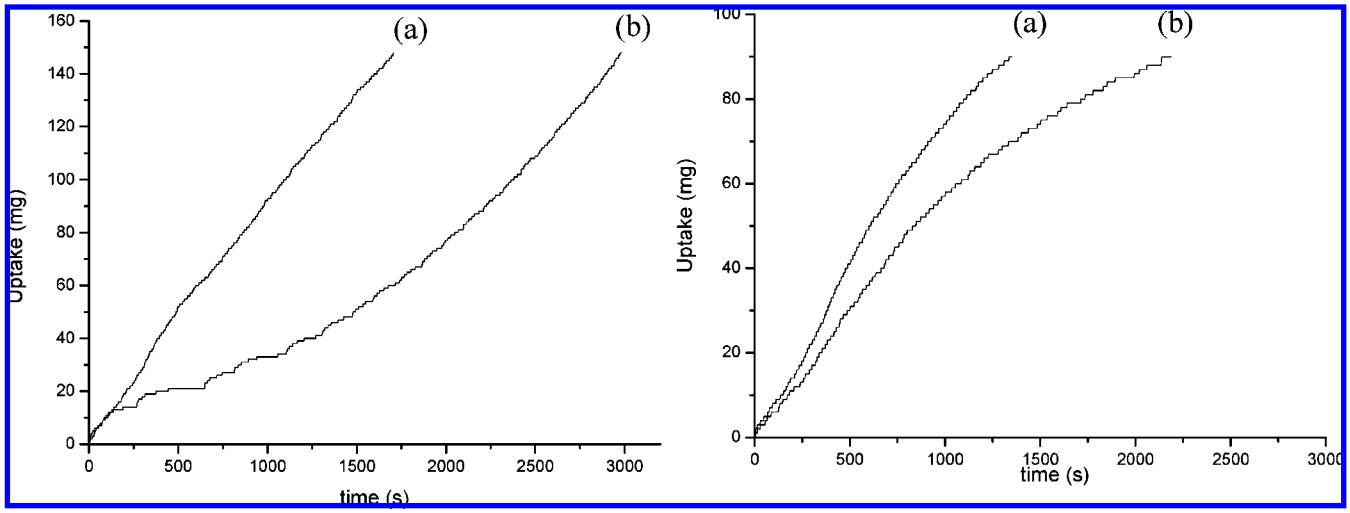

Figure 10. Results of propene polymerization at 50 °C in toluene for catalyst systems derived from precatalyst **1b** (left) and **2** (right): (a) activation with $[CPh_3][B(C_6F_5)_4]$ and (b) activation with $[HNMe_2Ph][B(C_6F_5)_4]$.

Scheme 7. Differences in Activation Chemistry of Naphthyl and Phenyl Precatalysts with Brønsted Acids

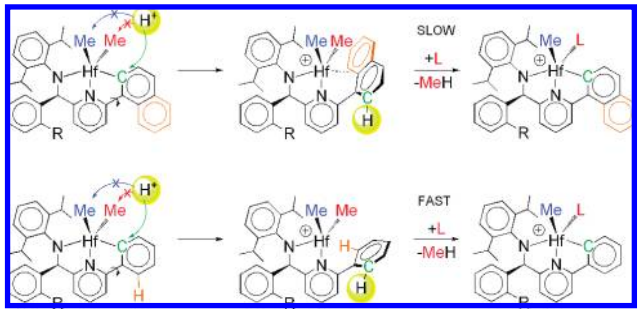

monomer, we are currently working to determine the selectivity of the first monomer insertion. These results, including detailed NMR characterization and computational studies, will be reported in the near future.

Experimental Section

All manipulations were performed in flamed Schlenk-type glassware interfaced to a high-vacuum line ($<10^{-5}$ Torr), or in a nitrogen-filled Vac-Atmosphere glovebox (<1 ppm O_2). Molecular sieves (MS) were activated for 24 h at 200−230 °C under dynamic vacuum. All the solvents and liquid reagents were freeze−pump−thaw degassed on the high-vacuum line, dried over the appropriate drying agent, vacuum-transferred to a dry storage-tube with a PTFE valve, and stored over activated MS. Benzene-d_6, toluene-d_8, pentane, hexane, and toluene were dried over Na/K alloy; 1,2-$F_2C_6H_4$ was refluxed for three days over P_2O_5, and finally dried over CaH_2, chlorobenzene-d_5 and methylene chloride-d_2 were dried over CaH_2.

$[HNMe_2Ph][B(C_6F_5)_4]$ and $[CPh_3][B(C_6F_5)_4]$ were obtained from Boulder Scientific Company and were used as received. $B(C_6F_5)_3$ was obtained from Boulder Scientific Company and was purified by sublimation (40−60 °C, 10^{-5} Torr). $NMe(C_{18}H_{37})_2$ (Aldrich) and $AlMe_3$ (22% in hexane, Akzo Nobel) were used as received. The pyridylamine ligands *N*-[2,6-diisopropylphenyl]-α-[2-methylphenyl]-6-(1-naphthalenyl)-2-pyridinemethanamine,[1] *N*-[2,6-diisopropylphenyl]-α-[2-isopropylphenyl]-6-(1-naphthalenyl)-2-pyridinemethanamine,[4b] and *N*-[2,6-diisopropylphenyl]-α-phenyl-6-(1-phenyl)-2-pyridinemethan-amine[1] were prepared as described previously.

NMR samples were prepared in oven-dried J-Young NMR tubes. ^1H, $^{13}C\{^1H\}$, ^1H COSY, ^1H NOESY, ^1H ROESY, ^1H,^{13}C HMQC, ^1H,^{13}C HMBC, ^{19}F, and ^{19}F,^1H HOESY NMR experiments were performed on a Bruker Avance DRX 400 instrument. Referencing by residual solvent signals is relative to TMS. Typical mixing time for the Overhauser experiments were in the range 120−800 ms.

General Synthesis of Hafnium Dimethyl Complexes. The desired precatalysts **1** and **2** were synthesized by reaction of the ligand with tetrakis(dimethylamido)hafnium (IV) followed by treatment with trimethylaluminum, as described previously.[1,4b] A representative procedure for **1a** is given below.

Synthesis of [*N*-[2,6-Diisopropylphenyl]-α-[2-methylphenyl]-6-(1-naphthalenyl)-2-pyridinemethanaminato] Hafnium Dimethyl (1a). A 27.5 g portion of *N*-[2,6-diisopropylphenyl]-α-[2-methylphenyl]-6-(1-naphthalenyl)-2-pyridinemethanamine (56.7 mmol) was dissolved in 100 mL of toluene, and a solution of tetrakis(dimethylamido) hafnium(IV) (20 g, 56.4 mmol) in toluene (50 mL) was slowly added to this solution dropwise over a period of 30 min. The reaction vessel was equipped with a condenser filled with activated acidic alumina to remove the liberated dimethylamine. The reaction was heated under reflux conditions for 1.5 h, and then stirred at room temperature for 16 h. Subsequently, the solution was subjected to a dynamic vacuum which reduced the volume of the solvent to ∼40 mL. To this solution, ∼35 mL of hexane were added and the mixture was stirred for 1 h before the precipitate was isolated by filtration on a glass frit. The precipitate was washed 3 times with ∼20 mL of pentane and then dried under dynamic vacuum. Another 50 mL of hexane were added to the filtrate, and it was stirred for another 2 h. This again led to the formation of a precipitate that was filtered off using a glass frit and, after washing 3 times with ∼20 mL of pentane, was dried under dynamic vacuum. The two precipitate fractions were combined, giving 30.5 g of the desired diamido complex (72.2% yield).

The diamido complex (20.0 g, 26.7 mmol) was dissolved in ∼80 mL of toluene, and 113 mL (226 mmol, 8.5 equiv.) of a solution of trimethylaluminum (2.0 M in hexane) was added over a period of 30 min. After 2.5 h of stirring at room temperature, the solvent volume was reduced under dynamic vacuum to ∼100 mL. The resulting precipitate was isolated by filtration and was washed 3 times with ∼20 mL of hexane before being dried under vacuum. The filtrate was reduced in volume to ∼30 mL, forming further precipitate which was again isolated on a frit, washed 3 times with ∼20 mL of hexane, and dried under vacuum. The two precipitate fractions were combined, giving 15.6 g of **1a** (85.1% yield). ^1H NMR (C_6D_6, 298 K, *J* values in Hz): δ 8.58 (d, $^3J_{HH} = 7.6$, H2), 8.26 (m, H8), 7.81 (d, $^3J_{HH} = 7.5$, H3), 7.72 (m, H5), 7.50 (d, $^3J_{HH} = 7.8$, H12), 7.29 (m, H6, H7 and H19), 7.17 (m, H28), 7.16 (m, H29), 7.09 (m, H27), 6.98 (d, $^3J_{HH} = 7.5$, H20), 6.91 (td, $^3J_{HH} = 7.3$, $^4J_{HH} = 1.4$, H21), 6.85 (d, $^3J_{HH} = 7.2$, H22), 6.82 (d, $^3J_{HH} =$

7.8, H13), 6.39 (s, H17), 6.36 (d, $^3J_{HH}$ = 7.8, H14), 3.80 (sept, $^3J_{HH}$ = 6.7, H31), 3.35 (sept, $^3J_{HH}$ = 6.7, H34), 1.85 (s, H24), 1.37 (d, $^3J_{HH}$ = 6.7, H32), 1.36 (d, $^3J_{HH}$ = 6.7, H36), 1.14 (d, $^3J_{HH}$ = 6.7, H35), 0.94 (s, H38), 0.70 (s, H37), 0.44 (d, $^3J_{HH}$ = 6.7, H33). $^{13}C\{^1H\}$ NMR (C_6D_6, 298K): δ 206.8 (s, C1), 170.9 (s, C15), 165.0 (s, C11), 148.0 (s, C26), 147.0 (s, C30), 146.5 (s, C25), 144.7 (s, C10 or C4) 143.3 (s, C18), 141.5 (s, C13), 136.7 (s, C23), 136.4 (s, C4 or C10), 134.8 (s, C2), 131.3 (s, C9), 130.63 (s, C5), 130.56 (s, C3), 130.4 (s, C19), 128.4 (s, buried under C_6D_6, C21), 127.9 (s, C20), 127.6 (s, C7), 127.3 (s, C9), 126.7 (s, C28), 126.2 (s, C6), 125.8 (s, C29), 125.0 (s, C27), 124.8 (s, C8), 121.1 (s, C12), 120.0 (s, C14), 78.7 (s, C16), 67.6 (s, C37), 63.3 (s, C38), 29.4 (s, C34), 28.8 (s, C31), 28.1 (s, C32), 26.6 (s, C36), 26.0 (s, C35), 24.6 (s, C33), 20.5 (s, C24). Anal. Calcd (found) for $C_{37}H_{40}HfN_2$: H, 5.83 (5.86); C, 64.29 (64.35); N, 4.05 (4.08).

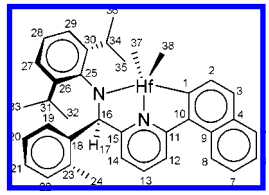

[*N*-[2,6-Diisopropylphenyl]-α-[2-isopropylphenyl]-6-(1-naphthalenyl)-2-pyridinemethanaminato] Hafnium Dimethyl (1b). ^1H NMR (C_6D_6, 298 K, *J* values in Hz): δ 8.60 (d, $^3J_{HH}$ = 7.6, H2), 8.25 (m, H8), 7.82 (d, $^3J_{HH}$ = 7.6, H3), 7.72 (m, H5), 7.50 (d, $^3J_{HH}$ = 7.9, H12), 7.31 (m, H6, H7 and H19), 7.16 (m, H28 and H29), 7.08 (m, H27 and H22), 7.00 (m, H20 and H21), 6.83 (d, $^3J_{HH}$ = 7.9, H13), 6.58 (s, H17), 6.55 (d, $^3J_{HH}$ = 7.9, H14), 3.83 (sept, $^3J_{HH}$ = 6.7, H31), 3.38 (sept, $^3J_{HH}$ = 6.7, H34), 2.90 (sept, $^3J_{HH}$ = 6.7, H24), 1.39 (d, $^3J_{HH}$ = 6.7, H36), 1.38 (d, $^3J_{HH}$ = 6.7, H32), 1.17 (d, $^3J_{HH}$ = 6.7, H24a), 1.16 (d, $^3J_{HH}$ = 6.7, H35), 0.96 (s, H38), 0.71 (s, H37), 0.70 (d, $^3J_{HH}$ = 6.7, H24b), 0.39 (d, $^3J_{HH}$ = 6.7, H33). $^{13}C\{^1H\}$ NMR (C_6D_6, 298 K): δ 206.7 (s, C1), 171.2 (s, C15), 165.0 (s, C11), 148.0 (s, C26), 147.4 (s, C23), 147.0 (s, C30), 146.2 (s, C25), 144.7 (s, C10) 141.5 (s, C18), 141.4 (s, C13), 136.4 (s, C4), 134.8 (s, C2), 131.4 (s, C9), 130.8 (s, C19), 130.6 (s, C5), 130.5 (s, C3), 128.8 (s, buried under C_6D_6, C21), 127.6 (s, C7), 127.5 (s, C20), 126.6 (s, C28), 126.2 (s, C6), 126.1 (C22), 125.8 (s, C29), 125.1 (s, C27), 124.9 (s, C8), 121.1 (s, C12), 120.1 (s, C14), 77.5 (s, C16), 67.6 (s, C37), 63.5 (s, C38), 29.4 (s, C34), 29.3 (s, C24), 28.8 (s, C31), 28.1 (s, C32), 26.5 (s, C36), 26.1 (s, C35), 25.8 (s, C24a), 24.4 (s, C33), 23.7 (s, C24b). Anal. Calcd (found) for $C_{39}H_{44}HfN_2$: H, 6.17 (6.23); C, 65.12 (65.15); N, 3.89 (3.85).

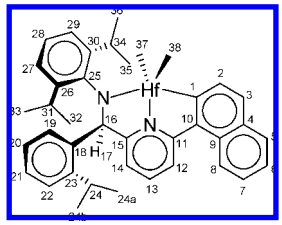

[*N*-[2,6-Diisopropylphenyl]-α-[phenyl]-6-(1-phenyl)-2-pyridinemethanaminato] Hafnium Dimethyl (2). H NMR (C_6D_6, 298 K, *J* values in Hz): δ 8.41 (d, $^3J_{HH}$ = 6.9, H2), 7.44 (d, $^3J_{HH}$ = 7.6, H9), 7.43 (dt, $^3J_{HH}$ = 7.4, $^4J_{HH}$ = 0.7, H3), 7.20 (dt, $^3J_{HH}$ = 7.6, $^4J_{HH}$ = 1.2, H4), 7.16 (m, buried under solvent signal H29,), 7.14 (t, $^3J_{HH}$ = 7.6, H28), 7.08 (dd, $^3J_{HH}$ = 7.4, $^4J_{HH}$ = 2.2, H27), 6.98 (m, H19, H20, H21; H22, H23) 6.89 (d, $^3J_{HH}$ = 7.8, H12), 6.79 (d, $^3J_{HH}$ = 7.8, H13), 6.36 (d, $^3J_{HH}$ = 7.8, H14), 5.90 (s, H17), 3.79 (sept, $^3J_{HH}$ = 6.7, H31), 3.21 (sept, $^3J_{HH}$ = 6.7, H34), 1.39 (d, $^3J_{HH}$ = 6.7, H32), 1.37 (d, $^3J_{HH}$ = 6.7, H36), 1.13 (d, $^3J_{HH}$ = 6.7, H35), 0.94 (s, H38), 0.62 (s, H37), 0.38 (d, $^3J_{HH}$ = 6.7, H33). $^{13}C\{^1H\}$ NMR (C_6D_6, 298K): δ 202.9 (s, C1), 170.1 (s, C15), 164.6 (s, C11), 148.1 (s, C26), 147.9 (s, C25), 147.2 (s, C30), 145.6 (s, C10) 144.7 (s, C18), 141.9 (s, C13), 139.2 (s, C2), 131.5 (s, C3), 129.7, 129.6 (s, C19, C20, C22, C23), 129.3 (s, C4), 128.6 (s, C21), 126.7 (s, C28), 125.8 (s, C29), 125.1 (s, C27), 124.0 (s, C9), 120.7 (s, C14), 116.4 (s, C12), 84.8 (s, C16), 67.7 (s, C37), 63.8 (s, C38), 29.3 (s, C34), 28.7 (s, C31), 27.7 (s, C32), 27.6 (s, C36), 25.5 (s, C35), 25.0 (s, C33). Anal. Calcd. (found) for $C_{32}H_{36}HfN_2$: H, 5.79 (5.81); C, 61.29 (61.29); N, 4.47 (4.45).

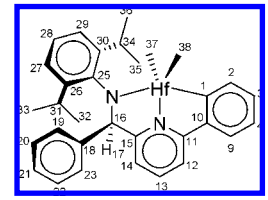

Synthesis of 3a. Complex **1a** (50 mg, 0.072 mmol) and $B(C_6F_5)_3$ (40 mg, 0.078 mmol) were loaded in the glovebox into the two separate vessels of a flip-frit reaction apparatus. The flip-frit was then interfaced to the high-vacuum line and evacuated to 10^{-5} Torr. Approximately 30 mL of dry pentane was condensed under vacuum at −196 °C into the vessel containing **1a**. The reaction vessel was then warmed to room temperature while stirring. After approximately $^1/_2$ h, the yellow solution was filtered into the second vessel containing $B(C_6F_5)_3$. A yellow solid precipitate formed almost instantaneously. Stirring was continued for an additional $^1/_2$ h and then the yellow solid was collected by filtration, rinsed once with a small amount of pentane, and dried under vacuum overnight. Yield: 50 mg (55%). H NMR(C_6D_6, 298 K, *J* values in Hz): δ 8.11 (d, $^3J_{HH}$ = 8.3, H8), 7.99 (d, $^3J_{HH}$ = 7.9, H2), 7.55 (d, $^3J_{HH}$ = 7.9, H3), 7.48 (d, $^3J_{HH}$ = 7.9, H5), 7.32 (d, $^3J_{HH}$ = 8.0, H12), 7.28 (td, $^3J_{HH}$ = 6.8, $^4J_{HH}$ = 1.5, H7), 7.18 (m, H6, H19, H28, and H20), 6.95 (dd, $^3J_{HH}$ = 7.7, $^4J_{HH}$ = 1.1, H27), 6.90 (t, $^3J_{HH}$ = 6.9, H21), 6.80 (dd, $^3J_{HH}$ = 7.7, $^4J_{HH}$ = 1.1, H29), 6.75 (d, $^3J_{HH}$ = 8.6, H22), 6.73 (t, $^3J_{HH}$ = 7.9, H13), 6.15 (d, $^3J_{HH}$ = 7.9, H14), 6.09 (s, H17), 3.22 (sept, $^3J_{HH}$ = 6.8, H31), 3.03 (br, Hf-Me-B), 2.70 (sept, $^3J_{HH}$ = 6.8, H34), 1.61 (s, H24), 1.12 (s, H38), 1.07 (d, $^3J_{HH}$ = 6.8, H36), 1.03 (d, $^3J_{HH}$ = 6.8, H32), 0.79 (d, $^3J_{HH}$ = 6.8, H35), 0.13 (d, $^3J_{HH}$ = 6.8, H33). ^{19}F NMR (C_6D_6, 298 K): δ −132.8 (br *o*-F), −159.2 (br, *p*-F), −163.9 (br, *m*-F). Anal. Calcd. (found) for $C_{55}H_{40}BF_{15}HfN_2$: H, 3.35 (3.40); C, 54.90 (54.97); N, 2.33 (2.27).

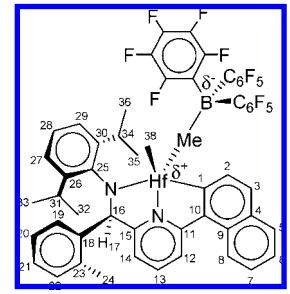

Synthesis of 3b. Complex **1b** (200 mg, 0.277 mmol) and $B(C_6F_5)_3$ (142.2 mg, 0.277 mmol) were loaded into one vessel of a flip-frit reaction apparatus within the glovebox. The flip-frit was interfaced to the high-vacuum line and evacuated up to 10^{-5} Torr. Approximately 25 mL of pentane was condensed under vacuum at −196 °C into the vessel containing the reactants. The reaction vessel was warmed up to approximately −20 °C and stirred for approximately 1 h at this temperature. The bright yellow solid that formed was collected by filtration, washed with a small amount of pentane, and dried under vacuum overnight. Yield: 240 mg (70%). ^1H NMR (C_6D_5Cl, 244 K, *J* values in Hz): δ 8.12 (m, H8), 7.84 (d, $^3J_{HH}$ = 7.8, H2), 7.56

(d, $^3J_{HH}$ = 7.8, H3), 7.51 (m, H5), 7.39 (d, $^3J_{HH}$ = 8.1, H12), 7.32 (m, H19, H6 and H7), 7.13 (m, H13 and H28), 7.06 (m, H20, H21 and H22), 6.92 (buried under residual solvent signals, H27), 6.82 (d, $^3J_{HH}$ = 7.6, H29), 6.61 (d, J_{HH} = 8.1, H14), 6.28 (s, H17), 3.28 (sept, $^3J_{HH}$ = 6.7, H31), 3.04 (br, Hf-Me-B), 2.86 (sept, $^3J_{HH}$ = 6.7, H34), 2.52 (sept, $^3J_{HH}$ = 6.7, H24), 1.19 (d, $^3J_{HH}$ = 6.7, H36), 1.14 (s, H38), 1.08 (d, $^3J_{HH}$ = 6.7, H24a), 0.99 (d, $^3J_{HH}$ = 6.7, H32), 0.76 (d, $^3J_{HH}$ = 6.7, H35), 0.47 (d, $^3J_{HH}$ = 6.7, H24b), 0.03 (d, $^3J_{HH}$ = 6.7, H33). Selected $^{13}C\{^1H\}$ NMR (C_6D_5Cl, 244 K): δ = 207.3 (s, C1), 170.4 (s, C15), 165.0 (s, C11), 142.3 (s, C13), 132.1 (s, C2), 130.1 (s, C3), 129.9 (s, C5), 124.4 (s, C8), 121.7 (s, C12), 120.8 (s, C14), 75.7 (s, C16), 65.8 (s, C38), 40.7 (s, Hf-Me-B), 26.4 (s, C32), 25.6 (s, C36), 25.4 (s, C24a), 25.0 (s, C35), 23.6 (s, C33), 22.3 (s, C24b). ^{19}F NMR (C_6D_5Cl, 244 K, J values in Hz): δ −132.70 (brd,$^3J_{FF}$ = 23.7, o-F), −158.90 (t, $^3J_{FF}$ = 21.3, p-F), −163.60 (brt, $^3J_{FF}$ = 23.3, m-F). ^{19}F NMR (C_6D_5Cl, 244 K, J values in Hz): δ −132.70 (brd, $^3J_{FF}$ = 23.7, o-F), −158.90 (t, $^3J_{FF}$ = 21.3, p-F), −163.60 (brt, $^3J_{FF}$ = 23.3, m-F). Anal. Calcd (found) for $C_{57}H_{44}BF_{15}HfN_2$: H, 3.60 (3.62); C, 55.60 (55.64); N, 2.28 (2.25).

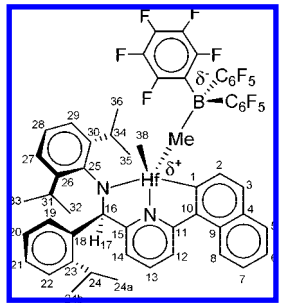

Synthesis of 5a. Complex **1a** (70 mg, 0.101 mmol) and $[HNMe_2Ph][B(C_6F_5)_4]$ (81 mg, 0.101 mmol) were loaded into a vessel of a flip-frit reaction apparatus within the glovebox. The flip-frit was then interfaced to the high-vacuum line and evacuated to 10^{-5} Torr. Approximately 20 mL of dry toluene were condensed under vacuum at −196 °C into the vessel. The reaction mixture was warmed up to room temperature and stirred approximately for 10 min. After that toluene was removed under vacuum and approximately 30 mL of dry pentane were condensed into the vessel. The initially formed deep yellow-brown oil was handled until a yellow solid was obtained. It was washed with a small amount of pentane and dried under high-vacuum overnight. Yield: 95 mg (68%). ^1H NMR (C_6D_6/1,2-$C_6H_4F_2$, 298 K, J values in Hz): δ 7.92 (td, $^3J_{HH}$ = 7.5, $^4J_{HH}$ = 1.3, H7), 7.75 (d, $^3J_{HH}$ = 7.9, H5), 7.72 (d, $^3J_{HH}$ = 7.8, H3), 7.61 (d, $^3J_{HH}$ = 7.6, H8), 7.50 (dd, $^3J_{HH}$ = 8.2, $^4J_{HH}$ = 7.2, H2), 7.49 (t, $^3J_{HH}$ = 7.8, H13), 7.32 (d, $^3J_{HH}$ = 7.6, H12), 7.23 (dd, $^3J_{HH}$ = 7.3, $^4J_{HH}$ = 1.0, H1), 7.18 (td, $^3J_{HH}$ = 7.3, $^4J_{HH}$ = 1.1, H6), 7.12 (dd, $^3J_{HH}$ = 7.8, $^4J_{HH}$ = 1.9, H29), 7.08 (t, $^3J_{HH}$ = 7.6, H28), 6.93 (m, H20 and H21), 6.84 (dd, $^3J_{HH}$ = 7.4, $^4J_{HH}$ = 1.9, H27), 6.79 (m, buried under 1,2-$C_6H_4F_2$, H22), 6.65 (d, $^3J_{HH}$ = 7.8, H14), 6.61 (d, $^3J_{HH}$ = 7.6, buried under 1,2-$C_6H_4F_2$, H19), 6.38 (s, buried under 1,2-$C_6H_4F_2$ side bands, H17), 3.08 (sept, $^3J_{HH}$ = 6.8, H34), 3.00 (sept, $^3J_{HH}$ = 6.8, H31), 1.71 (s, H24), 1.45 (d, $^3J_{HH}$ = 6.8, H36), 1.36 (d, $^3J_{HH}$ = 6.8, H35), 0.88 (d, $^3J_{HH}$ = 6.8, H32), 0.08 (d, $^3J_{HH}$ = 6.8, H33), −0.29 (s, H38), −0.50 (s, H37). Cation $^{13}C\{^1H\}$ NMR (C_6D_6/1,2-$C_6H_4F_2$, 298 K): δ 168.6 (s, C15), 153.1 (s, C11), 147.1 (s, C26), 145.5 (s, C30), 145.4 (s, C13), 143.9 (s, C7), 140.8 (s, C25), 139.7 (s, C23 or C18), 138.7 (s, C4), 138.1 (s, C18 or C23), 137.9 (s, C5), 134.0 (s, C3), 133.6 (s, C1), 132.1 (s, C22), 131.9 (s, C2), 131.7 (s, C6), 130.7 (s, C10), 130.1 (s, C19), 129.8 (s, C20 or C21), 128.6 (s, C9), 128.0 (s, C21 or C20), 126.1 (s, C29), 125.8 (s, C27), 125.4 (s, C14), 125.0 (s, C28), 123.1 (s, C12), 114.1 (s, C8), 75.1 (s, C16), 73.4 (s, C37), 61.8 (s, C38), 30.1 (s, C34), 29.0 (s, C31), 26.4 (s, C32), 26.2 (s, C35), 25.9 (s, C36), 24.0 (s, C33), 19.9 (s, C24). ^{19}F NMR (C_6D_6/1,2-$C_6H_4F_2$, 298 K, J values in Hz): δ −132.40 (br, o-F), −163.24 (t, $^3J_{HH}$ = 21.0, p-F), −167.13 (brt, $^3J_{HH}$ = 17.2, m-F). Anal. Calcd. (found) for $C_{61}H_{41}BF_{20}HfN_2$: H, 3.01 (3.12); C, 53.43 (53.55); N, 2.04 (2.12).

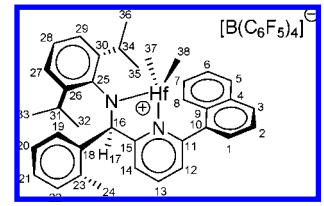

Synthesis of 5b. Complex **1b** (100 mg, 0.139 mmol) and $[HNMe_2Ph][B(C_6F_5)_4]$ (111.4 mg, 0.139 mmol) were loaded into a vessel of a flip-frit reaction apparatus within the glovebox. The flip-frit was then interfaced to the high-vacuum line and evacuated to 10^{-5} Torr. Approximately 20 mL of toluene were condensed under vacuum at −196 °C into the vessel. The reaction mixture was warmed up to room temperature and stirred approximately for 10 min. After that, toluene was removed under vacuum and approximately 30 mL of pentane were condensed into the vessel. The initially formed yellow oil was handled until a light yellow solid was obtained. It was washed with a small amount of pentane and dried under vacuum overnight. Yield: 150 mg (76%). Single crystals suitable for X-ray analysis were grown by slow diffusion of n-hexane into a concentrated solution of ion pair **5b** in C_6D_5Cl. The crystals belong to the $P\bar{1}$ space group with two ion pairs in each unit cell. ^1H NMR (C_6D_5Cl, 298 K, J values in Hz): δ 8.06 (td, $^3J_{HH}$ = 7.1, $^4J_{HH}$ = 1.3, H7), 7.95 (d, $^3J_{HH}$ = 8.5, H5), 7.90 (d, $^3J_{HH}$ = 8.4, H3), 7.81 (d, $^3J_{HH}$ = 8.1, H8), 7.63 (dd, $^3J_{HH}$ = 8.3, $^4J_{HH}$ = 7.3, H2), 7.59 (t, $^3J_{HH}$ = 8.0, H13), 7.46 (d, $^3J_{HH}$ = 8.0, H12), 7.44 (dd, $^3J_{HH}$ = 7.3, $^4J_{HH}$=1.1, H1), 7.39 (td, $^3J_{HH}$ = 7.2, $^4J_{HH}$ = 1.1, H6), 7.14 (dd, $^3J_{HH}$ = 7.7, $^4J_{HH}$ = 1.6, H29), 7.07 (t, $^3J_{HH}$ = 7.8, H28), 7,06 (m, H22), 7.00 (m, H21 and H20), 6.92 (d, $^3J_{HH}$ = 8.0, H14), 6.85 (dd, $^3J_{HH}$ = 7.4, $^4J_{HH}$ = 1.9, H27), 6.67 (d, $^3J_{HH}$ = 7.8, H19), 6.57 (s, H17), 3.11 (sept, $^3J_{HH}$ = 6.8, H34), 3.00 (sept, $^3J_{HH}$ = 6.8, H31), 2.59 (sept, $^3J_{HH}$ = 6.8, H24), 1.47 (d, $^3J_{HH}$ = 6.8, H36), 1.36 (d, $^3J_{HH}$ = 6.8, H35), 1.15 (d, $^3J_{HH}$ = 6.8, H24a), 0.88 (d, $^3J_{HH}$ = 6.8, H32), 0.5 (d, $^3J_{HH}$ = 6.8, H35), 0.08 (d, $^3J_{HH}$ = 6.8, H33), −0.25 (s, H38), −0.49 (s, H37). Cation $^{13}C\{^1H\}$ NMR ((C_6D_5Cl, 298 K, 298 K): δ 168.3 (s, C15), 152.2 (s, C11), 148.0 (s, C26), 146.4 (s, C30), 144.6 (s, C25), 144.4 (s, C13), 143.0 (s, C7), 139.2 (s, C23 or C18), 137.9 (s, C4), 137.2 (s, C5), 136.9 (s, C18 or C23), 133.3 (s, C3), 132.9 (s, C1), 131.3 (s, C2), 131.0 (s, C6), 129.9 (s, C10), 129.7 (s, C19), 129.5 (s, C21 or C22), 128.8 (s, C28), 127.7 (s, C9), 126.9 (s, C20), 126.3 (s, C22 or C21), 125.4 (s, C29), 125.2 (s, C27), 124.4 (s, C14), 122.3 (s, C12), 113.3 (s, C8), 73.0 (s, C16), 72.9 (s, C37), 61.8 (s, C38), 29.3 (s, C34), 28.7 (s, C24), 28.2 (s, C31), 25.82 (s, C32), 25.78 (s, C35), 25.1 (s, C24a), 25.0 (s, C36), 23.2 (s, C33), 22.3 (s, C24b). ^{19}F NMR (C_6D_6Cl, 298 K, J values in Hz): δ −132.2 (br, o-F), −162.6 (t, $^3J_{FF}$ = 21.0, p-F), −166.6 (brt, $^3J_{FF}$ = 19.0, m-F). Anal. Calcd. (found) for $C_{63}H_{45}BF_{20}HfN_2$: H, 3.24 (3.30); C, 54.07 (54.15); N, 2.00 (2.06).

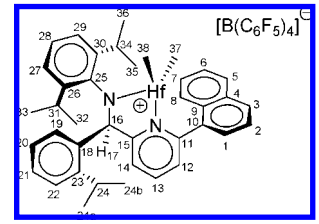

Generation of complex 6a. Complex **5a** (7.5 mg, 0.0055 mmol) and $[HNMe_2Ph][B(C_6F_5)_4]$ (4.4 mg, 0.0055 mmol) were loaded into a 2 mL vial within the glovebox. One milliliter of C_6D_6 was added. The vial was closed with a screw cap, shaken several times during the first two hours, and left overnight at room temperature. A deep

yellow-brown oil separated from the solution. The supernatant solution was removed, and the residual oil was washed with C_6D_6 (2 × 0.3 mL). The same procedure was repeated starting directly from **1a** and using 2 equiv of $[HNMe_2Ph][B(C_6F_5)_4]$. NMR analysis indicated that the final product was the same but of lower purity. ^{1}H NMR (CD_2Cl_2, 217 K, *J* values in Hz): δ 8.66 (d, $^3J_{HH}$ = 8.3, H3), 8.48 (t, $^3J_{HH}$ = 7.9, H13), 8.41 (d, $^3J_{HH}$ = 7.7, H5), 8.37 (d, $^3J_{HH}$ = 7.8, H8), 8.21 (d, $^3J_{HH}$ = 7.8, H12), 8.10 (m, H6 and H7), 7.99 (dd, $^3J_{HH}$ = 8.2, $^4J_{HH}$ = 6.3, H2), 7.60 (d, $^3J_{HH}$ = 8.0, H14), 7.48 (d, $^3J_{HH}$ = 6.3, H1), 7.42 (d, $^3J_{HH}$ = 7.6, H29), from 7.40 to 7.10 series of multiplets in the following order H28, H21, H20, H19, H22, H27, and *m*-H, 6.61 (dd, $^3J_{HH}$ = 8.3, $^4J_{HH}$ = 2.3, *o*-H), 6.17 (s, H17), 5.75 (brd, *o*-H′), 5.72 (t, $^3J_{HH}$ = 7.1, *p*-H), 5.03 (td, $^3J_{HH}$ = 8.3,$^4J_{HH}$ = 1.5, *m*-H′), 3.23 (s, H39), 2.81 (sept, $^3J_{HH}$ = 6.5, H34), 2.72 (sept, $^3J_{HH}$ = 6.5, H31), 2.60 (s, H40), 2.81 (sept, $^3J_{HH}$ = 6.5, H34), 1.87 (s, H24), 1.51 (d, $^3J_{HH}$ = 6.5, H36), 1.50 (s, H38), 1.32 (d, $^3J_{HH}$ = 6.5, H35), 0.97 (d, $^3J_{HH}$ = 6.5, H32), 0.02 (d, $^3J_{HH}$ = 6.5, H33). Cation ^{13}C{^{1}H} NMR (CD_2Cl_2, 217 K): δ 167.9 (s, C15), 153.3 (s, C11), 152.8 (s, C*ipso*) 147.4 (s, C13), 147.0 (s, C26), 142.7 (s, C25), 142.3 (s, C30), 138.2 (s, C18), 136.8 (s, C3), 136.79 (s, C4), 135.7 (s, C23), 135.4 (s, *m*-C′), 134.7 (*m*-C), 133.4 (s, C6 and C10), 133.0 (s, C7), 132.9 (s, C22), 131.2 (s, C5), 130.2 (s, C2 and C20), 130.0 (s, C28), 129.6 (s, C19), 129.3 (s, C9), 128.2 (s, C21), 127.6 (s, C29), 127.2 (s, C12), 126.7 (s, C27), 125.0 (s, C14) 124.6 (s, C8), 122.7 (s, C1), 114.8 (s, *o*-C), 111.6 (s, *o*-C′), 107.9 (s, *p*-C), 73.7 (s, C16), 56.9 (S, C38), 41.4 (s, C39), 40.9 (s, C40), 28.8 (s, C34), 28.6 (s, C31), 27.3 (s, C36), 26.3 (s, C32), 25.2 (s, C35), 23.9 (s, C33), 20.8 (s, C24). ^{19}F NMR (CD_2Cl_2, 217 K, *J* values in Hz): δ −133.70 (brd, *o*-F), −163.00 (t, $^3J_{FF}$ = 21.0, *p*-F), −167.09 (brt, $^3J_{FF}$ = 17.8, *m*-F).

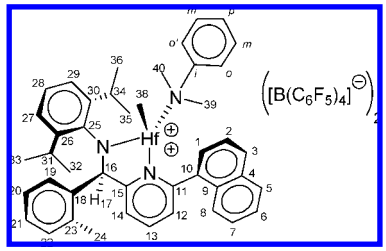

Generation of Complexes 7b and 8b. Complex **1b** (25 mg, 0.035 mmol) and $[HNMe_2Ph][B(C_6F_5)_4]$ (27.8 mg, 0.035 mmol) were loaded into a J-Young NMR tube within the glovebox and approximately 0.6 mL of C_6D_5Cl were added. After 56 h at room temp the solution changed color from light-yellow to deep-yellow, while a mixture containing **7b** (ca. 80%), **1b**, and other minor species was obtained.

7b. ^{1}H NMR (C_6D_5Cl, 251 K, J values in Hz): δ 8.11 (m, H8), 7.98 (d, $^3J_{HH}$ = 8.3, H3), 7.94 (m, H5), 7.73 (d, $^3J_{HH}$ = 6.9, H1), 7.68 (m, H6 and H7), 7.56 (dd, $^3J_{HH}$ = 8.3, $^3J_{HH}$ = 6.9, H2), 7.46 (m, H19, H12 and H13), 7.28 (m, H20, H21 and H22), 7.17 (m, H27, H28 and H14), 6.98 (m, H29 and *m*-H), 6.77 (t, $^3J_{HH}$ = 7.3, *p*-H), 6.70 (d, $^3J_{HH}$ = 8.1, *o*-H), 6.60 (s, H17), 6.21 (dd, $^3J_{HH}$ = 7.3, $^4J_{HH}$ = 1.3, *m*-H′), 3.88 (sept, $^3J_{HH}$ = 6.8, H31), 2.89 (sept, $^3J_{HH}$ = 6.8, H24), 2.57 (sept, $^3J_{HH}$ = 6.8, H34), 2.13 (s, H40), 1.48 (d, $^3J_{HH}$ = 6.8, H32), 1.41 (d, $^3J_{HH}$ = 6.8, H36), 1.40 (s, H38), 1.32 (d, $^3J_{HH}$ = 6.8, H24a), 0.86 (s, H39), 0.64 (d, $^3J_{HH}$ = 6.8, H24b), 0.40 (d, $^3J_{HH}$ = 6.8, H33), −0.09 (d, $^3J_{HH}$ = 6.8, H35). Selected ^{13}C{^{1}H} NMR signals (C_6D_5Cl, 251 K): δ 192.9 (s, *o*-C′), 170.5 (s, C15), 155.8 (s, C11), 153.2 (s, C*ipso*), 141.8 (s, C13), 134.8 (s, *m*C′), 134.1 (s, C3), 132.8 (s, *m*C), 130.5 (s, C5), 130.1 (buried under solvent signal, C6 and C7), 128.9 (s, *p*C), 127.7 (s, C2), 127.6 (s, C1), 124.5 (s, C14), 124.1 (s, C8), 117.2 (s, *o*C), 73.7 (s, C17), 66.7 (s, C38), 46.5 (s, C40), 44.1 (s, C39), 29.3 (s, C34), 29.2 (s, C24), 28.8 (s, C31), 26.8 (s, C32), 26.0 (s, C36), 24.9 (s, C24a), 24.0 (s, C33), 23.2 (s, C24b), 22.6 (s, C35). ^{19}F NMR (C_6D_5Cl, 251 K, *J* values in Hz): δ −132.10 (br, *o*-F), −162.7 (t, $^3J_{HH}$ = 20.6, *p*-F), −166.60 (brt, $^3J_{HH}$ = 17.9, *m*-F). After seven days at room temperature, the solution changed its color from deep-yellow to light-orange. The complete consumption of ion pair **7b** was observed, while mixture containing approximately 75% of **8b** was obtained.

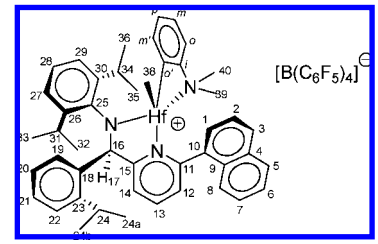

8b. ^{1}H NMR (C_6D_5Cl, 298 K, *J* values in Hz): δ 8.34 (d, $^3J_{HH}$ = 8.5, H8), 7.83 (d, $^3J_{HH}$ = 7.3, H12), 7.81 (d, $^3J_{HH}$ = 7.9, H5), 7.63 (d, $^3J_{HH}$ = 7.7, H3), 7.58 (td, $^3J_{HH}$ = 8.5, $^4J_{HH}$ = 1.0, H7), 7.496 (d, $^3J_{HH}$ = 7.7, H2), 7.492 (m, H6), 7.46 (d, $^3J_{HH}$ = 7.9, H13), 7.30 (d, $^3J_{HH}$ = 7.1, H29), 7.22 (m, H28), 7.13−7.04 (m, H22, H21 and H27), 7.03 (s, H17), 6.93 (d, $^3J_{HH}$ = 8.3, H14), 6.90 (t, $^3J_{HH}$ = 7.4, H20), 6.71 (m, H19 and *m*-H), 6.13 (d, $^3J_{HH}$=7.9, *o*-H), 6.11 (t, $^3J_{HH}$=7.7, *p*-H), 3.23 (sept, $^3J_{HH}$=6.6, H34), 3.13 (sept, $^3J_{HH}$ = 6.6, H24), 2.96 (m, H31), 2.37 (s, H39 or H40), 1.96 (s, H40 or H39), 1.68 (d, $^3J_{HH}$ = 6.6, H36), 1.38 (m, H32a), 1.32 (d, $^3J_{HH}$ = 6.6, H35), 1.24 (d, $^3J_{HH}$ = 6.6, H24a), 1.01 (d, $^3J_{HH}$ = 6.6, H33), 0.78 (m, H32b), 0.63 (d, $^3J_{HH}$ = 6.6, H24b). Selected cation ^{13}C{^{1}H} NMR signals (C_6D_5Cl, 298 K): δ 206.1 (s, C1), 170.8 (s, C15), 162.4 (s, C11), 150.3 (s, C26), 147.9 (s, C23), 146.6 (s, C*ipso*), 146.2 (s, C30), 142.6 (s, C13), 142.3 (s, C10) 141.1 (s, C25), 139.4 (s, C18), 135.4 (s, C4), 132.3 (s, *m*-C) 132.1 (s, C2), 130.8 (s, C9), 129.9 (s, C5), 128.6−128.1 (buried under solvent signal, C3, C7, C19 and C21), 127.7 (s, C28), 127.0 (s, C6), 126.7 (s, C20), 126.1 (buried under solvent signal, C22 and C29), 124.0 (s, C27), 123.7 (C8), 121.0 (s, C12), 119.7 (s, C14), 116.9 (s, *p*-C), 113.8 (s, *o*-C), 81.2 (s, C32), 75.8 (s, C16), 41.3 (s, C39 or C40), 40.4 (s, C40 or C39), 36.2 (s, C31), 28.8 (s, C24), 28.0 (s, C34), 26.1 (s, C35), 26.0 (s, C33), 25.5 (s, C24a), 25.0 (s, C36), 22.3 (s, C24b). ^{19}F NMR (C_6D_5Cl, 298 K, *J* values in Hz): δ −131.9 (br, *o*-F), −163.1 (t, $^3J_{HH}$ = 19.9, *p*-F), −166.90 (brt, $^3J_{HH}$ = 18.1, *m*-F).

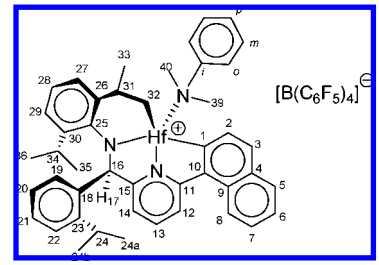

Generation of Complex 9b. Complex **5b** (20 mg, 0.0143 mmol) and $CH_3N(C_{18}H_{37})_2$ (7.7 mg, 0.0144 mmol) were weighted inside a J-Young NMR tube and approximately 0.7 mL of C_6D_5Cl were added at room temperature inside the glovebox. The reaction was followed by NMR as described in the text, affording complex **9b** quantitatively after 1 h at room temperature. ^{1}H NMR(C_6D_5Cl, 298 K, *J* values in Hz): δ 8.30 (d, $^3J_{HH}$ = 8.5, H8), 8.16 (d, $^3J_{HH}$ = 7.9, H2), 7.90 (d, $^3J_{HH}$ = 7.9, H3), 7.79 (d, $^3J_{HH}$ = 8.3, H5), 7.72 (d, $^3J_{HH}$ = 8.0, H12), 7.53 (m, H7), 7.43 (m, H6), 7.35 (t, $^3J_{HH}$ = 7.9, H13), 7.20−7.00 (m, H19, H20, H21, H22, H27, H28, H29), 6.74 (d, $^3J_{HH}$ = 7.8, H14), 6.64 (s, H17), 3.37 (sept, $^3J_{HH}$ = 6.6, H31), 2.88 (sept, $^3J_{HH}$ = 6.6, H34), 2.59 (m, H24 and NCH_2-), 2.35 (m, NCH_2-), 2.33 (s, NCH_3), 2.21 (m, NCH_2-), 1.48 (s, H38), 1.44 (d, $^3J_{HH}$ = 6.6, H36), 1.35−1.20 (m, (-CH_2-)$_n$), 1.14 (m, H24a, H33, H35), 0.88 (t, $^3J_{HH}$ = 7.0, CH_2CH_3), 0.57 (d, $^3J_{HH}$ = 6.6, H24b), 0.14 (d, $^3J_{HH}$ = 6.6, H32). Selected ^{13}C{^{1}H} NMR (C_6D_5Cl, 298 K): δ 202.2 (s, C1), 170.3 (s, C15), 163.8 (s, C11), 147.4 (s, C26), 147.1 (s, C23), 145.2 (s, C25), 144.5 (s, C10), 144.3 (s, C30), 143.5 (s, C13), 138.9 (s, C18), 135.8 (s, C4), 131.5 (s, C2), 131.2 (s, C3), 130.0 (s, C5), 129.8 (s, C9), 128.9 (s, C7), 127.6 (s, C6), 123.7 (s, C8), 121.1 (s, C12), 120.4 (s, C14), 77.1 (s, C16), 71.7 (s, C38), 54.4 (s, NCH_2-), 53.9 (s, NCH_2-), 40.3 (s, NCH_3), 32.0−24.0 (several signals corresponding to the (-CH_2-)$_n$, the main signal is centered at 30.1 ppm), 28.7 (s, C24), 28.11 (s, C34) 28.07 (s, C31), 27.0, 26.0, 25.1 (C24a, C33, C35), 26.6 (S, C36), 24.0

(s, C32), 22.6 (s, C24b), 14.3 (s, CH_2CH_3). ^{19}F NMR (C_6D_5Cl, 298 K, J values in Hz): δ −132.24 (br, *o*-F), −162.95 (t, $^3J_{HH}$ = 20.8, *p*-F), −166.75 (brt, $^3J_{HH}$ = 18.5, *m*-F).

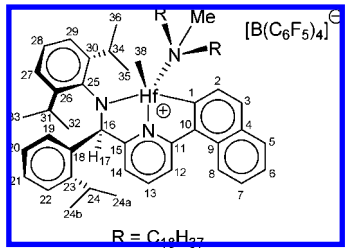

Generation of Complex 12. Complex **2** (20 mg, 0.032 mmol) and $[HNMe_2Ph][B(C_6F_5)_4]$ (25.5 mg, 0.032 mmol) were loaded in two separate vials inside the glovebox. C_6D_5Cl was added to both vials; the solutions were mixed and then transferred into a J-Young NMR tube. Evolution of gas was instantaneously observed inside the NMR tube. After 40 min a mixture of **11** and **11′** was obtained as described in the text. Leaving the NMR tube at room temperature for approximately 6 h or, alternatively, gently warming it for 2−4 min caused the quantitative formation of **12**. $_1$H NMR(C_6D_5Cl, 298 K, J values in Hz): δ 7.60 (d, $^3J_{HH}$ = 7.5, H9), 7.44 (t, $^3J_{HH}$ = 7.3, H13), 7.40 (d, $^3J_{HH}$ = 7.4, H12), 7.25 (m, H3, H4, H29, H2), 7.12 (t, $^3J_{HH}$ = 7.7, H28), 6.99 (t, $^3J_{HH}$ = 7.2, H21), 6.91 (m, H20 and H27), 6.82 (m, H14, H19 and *m*-H), 6.57 (s, H17), 6.10 (d, $^3J_{HH}$ = 8.7, *o*-H), 6.01 (t, $^3J_{HH}$ = 7.1, *p*-H), 3.26 (m, H31), 3.10 (sept, $^3J_{HH}$ = 6.7, H34), 2.37 (s, H39 or H40), 2.11 (s, H40 or H39), 1.68 (d, $^3J_{HH}$ = 6.7, H36), 1.33 (d, $^3J_{HH}$ = 6.7, H35), 1.26 (dd, $^2J_{HH}$ = 14.4,$^3J_{HH}$ = 13.2, H32b), 0.97 (d, $^3J_{HH}$ = 6.6, H33), 0.37 (dd, $^2J_{HH}$ = 14.4,$^3J_{HH}$ = 4.7, H32b). Cation ^{13}C{^{1}H} NMR (C_6D_5Cl, 298 K): δ 197.0 (s, C1), 169.9 (s, C15), 163.1 (s, C11), 151.0 (s, C26), 148.8 (s, C_{ipso}), 146.8 (s, C10), 146.4 (s, C30), 143.3 (s, C13), 142.0 (s, C18) 141.1 (s, C25), 138.0 (s, C2), 132.5 (s, *m*-C) 130.2 (s, C3), 129.9 (s, C4), 129.0 (s, C20, C22), 128.8 (s, C21), 128.4 (s, C19, C23), 127.5 (s, C28), 126.1 (s, C29), 125.0 (s, C9), 123.9 (s, C27), 121.1 (s, C14), 117.0 (s, C12), 114.5 (s, *p*-C), 113.3 (s, *o*-C), 82.5 (s, C32), 80.5 (s, C16), 40.5 (s, C39 or C40), 40.4 (s, C40 or C39), 36.8 (s, C31), 28.6 (s, C34), 26.34 (s, C36), 26.30 (s, C33), 25.1 (s, C35). ^{19}F NMR (C_6D_5Cl, 298 K, J values in Hz): δ −132.2 (br, *o*-F), −162.7 (t, $^3J_{HH}$ = 21.0, *p*-F), −166.6 (brt, $^3J_{HH}$ = 18.5, *m*-F).

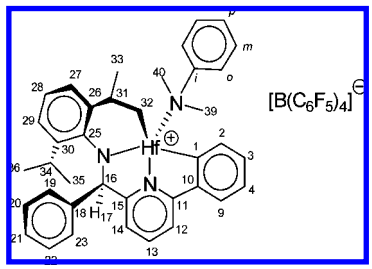

X-ray Crystallographic Analysis. Details of the analysis are included in the Supporting Information.

General Procedure for 1-Octene Polymerization. In a glovebox under inert atmosphere, a 40 mL vial was loaded with a magnetic stir bar and was placed into a foam block to minimize ambient heat loss. The vial was loaded with 1-octene (10 mL), catalyst, precatalyst, and enough toluene to give a final total volume of 20 mL. The vial was fitted with a septum cap and a thermocouple connected to a datalogging thermometer was introduced to record the temperature of the reaction medium. The polymerization was initiated by addition of the desired cocatalyst (1 equiv), and the temperature was recorded until it began to decrease. Further details of the specific polymerization experiments are given in the Supporting Information.

General Procedure for Propene Polymerization. Polymerization experiments were carried out with a high throughput parallel reactor setup (PPR24 available from Symyx Technologies, Inc.), with three reactor modules each containing eight reaction cells (6 mL working volume per cell). The whole system is housed in a triple MBraun LabMaster glovebox maintaining a pure nitrogen atmosphere (oxygen and water levels <1 ppm_v). The monomer gas and quench gas lines are plumbed directly into the reactors and controlled by automatic valves. Liquid reagents are robotically added to individual cells by syringes. For the purpose of this work, one eight-cell reactor was used (four experiments in duplicate) according to the following procedure. The cells are fitted with a preweighed glass vial insert and a disposable stirring paddle. The reactor is then closed, and 0.25 mL of a 0.020 M solution of ^{i}Bu$_3$Al in toluene and 3.95 mL of toluene are injected into each cell through a valve. The reactor temperature is set to 50 °C, and stirring is started at a speed of 800 rpm. The reactor is pressurized at 2.0 bar (30 psi) with nitrogen and then an overpressure of 2.0 bar (30 psi) of propene is applied. In an array of 8 × 1.2 mL glass vials positioned on a vortexer, precatalyst, and activator are premixed immediately prior to addition to the cells. To each vial, 0.890 mL of toluene, 0.050 mL of a 4.0 mM precatalyst solution in toluene, and 0.060 mL of a 4.0 mM activator solution in toluene are added. Aliquots of the resultant solutions are then injected into the cells (50 μL for activation with $[CPh_3][B(C_6F_5)_4]$, 250 μL for activation with $[HNMe_2Ph][B(C_6F_5)_4]$). In each cell the polymerization is run at constant temperature and propene partial pressure until a predetermined propene uptake is reached (typically, 100−150 mg), at which point the reaction is quenched with air at 3.4 bar (50 psi) overpressure. The reactor is opened, and the glass inserts are unloaded from the cells, transferred to a centrifuge/vacuum drying unit (Genevac EZ-2 Plus), and dried to constant weight, after which the polymer samples are recovered and weighed. Reproducility of polymer yield for experiments run is duplicate is typically better than ±20%.

Acknowledgment. We thank the Ministero dell'Università e della Ricerca (MUR, Rome, Italy) and The Dow Chemical Company for support.

Supporting Information Available: Computational details, additional NMR data, and X-ray crystallographic characterization of complex **5b**. This material is available free of charge via the Internet at http://pubs.acs.org.

JA802072N